Tectonics®

RESEARCH ARTICLE
10.1029/2021TC006889

Key Points:

- High-pressure/low-temperature parageneses, related to the M1 conditions, in the Alpujárride Complex dated at 38 Ma by $^{40}Ar/^{39}Ar$ of white micas
- Later retrograde micas yield a 20 Ma spike extensively recorded throughout the Betic Cordillera, and corresponds to a regional exhumation
- En-masse isothermal decompression forced the Ar-white mica system into the open-system *P-T* field producing a resetting of $^{40}Ar/^{39}Ar$ ages

Supporting Information:

Supporting Information may be found in the online version of this article.

Correspondence to:

E. Bessière,
eloise.bessiere@gmail.com

Citation:

Bessière, E., Scaillet, S., Augier, R., Jolivet, L., Miguel Azañón, J., Booth-Rea, G., et al. (2022). $^{40}Ar/^{39}Ar$ age constraints on H*P*/L*T* metamorphism in extensively overprinted units: The example of the Alpujárride subduction complex (Betic Cordillera, Spain). *Tectonics*, *41*, e2021TC006889. https://doi.org/10.1029/2021TC006889

Received 5 MAY 2021
Accepted 15 DEC 2021

Author Contributions:

Conceptualization: Eloïse Bessière
Data curation: Eloïse Bessière, Romain Augier, Laurent Jolivet, Adrien Romagny
Formal analysis: Eloïse Bessière, Stéphane Scaillet
Funding acquisition: Laurent Jolivet
Investigation: Eloïse Bessière, Romain Augier, Laurent Jolivet, Jose Miguel Azañón, Guillermo Booth-Rea, Adrien Romagny
Methodology: Stéphane Scaillet, Florian Duval

$^{40}Ar/^{39}Ar$ Age Constraints on H*P*/L*T* Metamorphism in Extensively Overprinted Units: The Example of the Alpujárride Subduction Complex (Betic Cordillera, Spain)

Eloïse Bessière[1,2,3,4], Stéphane Scaillet[2,3,4], Romain Augier[2,3,4], Laurent Jolivet[1], Jose Miguel Azañón[5,6], Guillermo Booth-Rea[5,6], Adrien Romagny[1], and Florian Duval[2,3,4]

[1]Sorbonne Université, CNRS-INSU, Institut des Sciences de la Terre Paris, ISTeP UMR, Paris, France, [2]Université d'Orléans, Institut des Sciences de la Terre d'Orléans (ISTO), UMR, Orléans, France, [3]CNRS/INSU, ISTO, UMR, Orléans, France, [4]BRGM, ISTO, UMR, Orléans, France, [5]Departamento de Geodinámica, Universidad de Granada, Granada, Spain, [6]Instituto Andaluz de Ciencias de la Tierra, CSIC-UGR, Granada, Spain

Abstract Widespread overprinting of early high-pressure/low-temperature (H*P*/L*T*) subduction stages due to subsequent collisional or late-orogenic tectono-metamorphic events is a common feature affecting the interpretation of geochronologic data from H*P*/L*T* orogens. The Betic-Rif orogen is exemplary in this connection as a great majority of published radiometric ages are found to cluster around 20 Ma. This clustering is commonly interpreted as reflecting a short, yet complex, succession of tectono-metamorphic events spanning only over a few Myr, including back-arc extension and overthrusting of the Internal Zones on the External Zones. An alternative explanation consists in the poor preservation of a much earlier H*P*/L*T* metamorphic event, presumably Eocene, coeval with subduction and crustal thickening in the Internal Zones, and particularly the Alpujárride Complex. However, this age is vividly debated due to widespread resetting by the Early Miocene H*T*/L*P* overprint. In this study, we provide new $^{40}Ar/^{39}Ar$ evidence from white micas selected along an E-W section of the Internal Betics, from the central to the eastern Alpujárride Complex. Our new data show (a) that exceptionally well-preserved H*P*/L*T* parageneses in this unit retain a well-defined Eocene age around 38 Ma, and (b) that widespread 20 Ma ages recorded all along the section correspond to a regional stage of exhumation, coeval with a major change in the kinematics of back-arc extension. Our study provides conclusive evidence that $^{40}Ar/^{39}Ar$ dating of carefully targeted H*P*/L*T* associations can overcome the problem of extensive late-orogenic overprinting, testifying for an Eocene H*P* event around 38 Ma in the Betic-Rif orogen.

1. Introduction

How the dynamics of subducting lithospheric slabs interferes with crustal deformation in the upper plates of convergence zones is a major question in plate-kinematic and crustal-scale restorations. This question is particularly well illustrated in the Betic-Rif orogen (western Mediterranean) which results from complex interactions between the Africa and Iberia plates during their convergence and deep-seated slab dynamics (Dewey et al., 1989; Faccenna et al., 2004, 2014; Jolivet et al., 2003; Lonergan & White, 1997; Mancilla et al., 2015; Platt et al., 2003; Spakman & Wortel, 2004). The arcuate bending of the orogen and drastic kinematic changes (Crespo-Blanc et al., 2016; Faccenna et al., 2014; Jolivet & Faccenna, 2000; Jolivet et al., 2003; Platt et al., 1998, 2013; Platt & Vissers, 1989; Vergés & Fernàndez, 2012) during the Miocene have led to a complex 3-D organisation and pressure-temperature-time (*P-T*-t) evolution that are important to decipher in order to understand the dynamics of such a complex system. Central to this question is the age of the high-pressure/low-temperature (H*P*-L*T*) event marking the subduction of large portions of the Internal Zones and the timing of the transition toward shallower crustal conditions during exhumation of the H*P* units.

Deciphering such dynamics is complex because early (deep-seated) metamorphic stages can be partially or even wholly overprinted during exhumation, obscuring the sequence of tectono-metamorphic events contributing to the finite structure of the exhumed crustal stack like in, for example, Himalayan, Aegean, the Alps, Alpine Corsica, the Zagros or the Menderes massif. To address this issue, several thermo-chronological methods (e.g., U/Pb on zircon, $^{40}Ar/^{39}Ar$ on white mica, fission-tracks in both zircon and apatite) are usually required in combination with detailed petrochronology, thermochronometers and structural data to properly constrain the timing of peak-metamorphic events and subsequent exhumation (e.g., Beaudoin et al., 2020; Dragovic et al., 2020; Kohn et al., 2017; Kurzawa et al., 2017; Laurent et al., 2021; Plunder et al., 2016).

Project Administration: Laurent Jolivet
Resources: Laurent Jolivet
Software: Stéphane Scaillet
Supervision: Stéphane Scaillet, Romain Augier, Laurent Jolivet, Jose Miguel Azañón, Guillermo Booth-Rea
Validation: Romain Augier, Laurent Jolivet
Writing – original draft: Eloïse Bessière

The Betic-Rif Cordillera (Figure 1) is a young and well-exposed orogen with a major, regional-scale, metamorphic event massively overprinting earlier H*P*/L*T* tectono-metamorphic events that, thus, remain poorly constrained. The tight curvature of the orogen and the presence of a steeply dipping slab below the Alboran basin formed in the back-arc region have been explained by slab retreat and tearing (Faccenna et al., 2004; Jolivet et al., 2008; Lonergan & White, 1997; Spakman & Wortel, 2004). Several metamorphic and tectonic stages have long been recognized, with contrasting kinematics, but their respective timing remains unclear (Augier, Agard et al., 2005; Azañón & Crespo-Blanc, 2000; Homonnay et al., 2018; López Sánchez-Vizcaíno et al., 2001; Michard et al., 2006; Monié et al., 1991, 1994; Platt et al., 2005, 2006; Sánchez-Rodríguez & Gebauer, 2000; Tubía & Gil Ibarguchi, 1991). A majority of published ages is found to cluster around 20 Ma both for the H*P*/L*T* event linked to the initial subduction phase, and the high-temperature/low-pressure (H*T*/L*P*) event due to subsequent slab roll-back and back-arc lithospheric extension. This clustering suggests that the H*P*/L*T* and H*T*/L*P* metamorphic events and associated exhumation history occurred in a very short time span (Homonnay et al., 2018; López Sánchez-Vizcaíno et al., 2001; Michard et al., 2006; Platt et al., 2006; Sánchez-Rodríguez & Gebauer, 2000; Tubía & Gil Ibarguchi, 1991). Thus, fast cooling rates >70–90°C/Ma (up to ∼350°C/Ma during the 20–18 Ma period) have been proposed for the different metamorphic units of the Betic-Rif Cordillera with exhumation rates of 3–12 mm/yr (López Sánchez-Vizcaíno et al., 2001; Monié et al., 1994; Platt et al., 2006; Sánchez-Rodríguez & Gebauer, 2000). Peak-pressure conditions range from ∼8–10 kbar to ∼20–22 kbar and peak-temperatures from ∼350°C to ∼580°C (Augier, Agard et al., 2005; Azañón, 1992; Azañón et al., 1998; Azañón & Goffé, 1997a, 1997b; Booth-Rea et al., 2002; Bouybaouene et al., 1995; Chalouan et al., 2008; de Jong, 2003; Goffé et al., 1989; Li & Massonne, 2018; López Sánchez-Vizcaíno et al., 2001; Martínez-Martínez & Azañón, 1997; Michard et al., 1997; Nijhuis, 1964; Santamaría-López et al., 2019; Tubía & Gil Ibarguchi, 1991). The H*T*/L*P* event is mainly characterized by a fast and large decompression and a moderate temperature increase leading to a low *P*/*T* gradient about ∼4 kbar for 400–600°C (Augier, Agard et al., 2005; Azañón & Crespo-Blanc, 2000; Azañón et al., 1993, 1997, 1998; Balanyá et al., 1997; Jabaloy et al., 1993; Nijhuis, 1964; Soto & Azañón, 1994). Notably, the first unconformably overlying sediments found mostly in the central and eastern part of the region are dated at ∼20.5 Ma (Serrano et al., 2006, 2007) indicating that a substantial amount of exhumation had already occurred by that time, at odds with the timing of the H*P*/L*T* metamorphic event estimated between 25 Ma and 18 Ma (Sánchez-Rodríguez & Gebauer, 2000; Tubía & Gil Ibarguchi, 1991). Others argue for a partial to total resetting of the early H*P*/L*T* record during later back-arc extension or delamination at ∼20 Ma (Augier, Agard et al., 2005; Jolivet et al., 2003; Michard et al., 2006; Monié et al., 1994; Platt et al., 2005, 2013). A few studies have documented an Eocene age for the H*P*/L*T* event in the Alpujárride Complex (Monié et al., 1991; Platt et al., 2005), consistent with unconformably overlying Oligocene conglomerates on top of deformed Eocene sediments in Sierra Espuña in the Malaguide Complex further north (Lonergan, 1993). However, the lack of accurate structural and metamorphic information on the setting and evolution of the dated samples precluded any definite conclusion. $^{40}Ar/^{39}Ar$ Eocene ages were also obtained on micas, mainly white micas, from the deeper nappe of the Nevado-Filabride Complex (Augier, Agard et al., 2005; Monié et al., 1991). These ages have been regarded as suspiciously old due to possible excess argon and discarded in favor of Early Miocene Lu/Hf ages on garnets and U/Pb ages on zircons thought to date the peak of pressure (de Jong, 2003; López Sánchez-Vizcaíno et al., 2001; Platt et al., 2006). Using in situ dating of monazite with electron microprobe, Li and Massonne (2018) recently obtained Eocene ages from the same unit, shedding a new light on this question and reopening the debate.

We build on these past studies to reevaluate the age of the H*P*-L*T* event in the Alpujárride Complex based on a fresh sampling strategy. If the 20 Ma is related to a late tectonic event and the age of the H*P*-L*T* metamorphism is indeed Eocene, then only the well-preserved H*P*-L*T* parageneses are likely to preserve the isotopic record of this early event. Finding such parageneses is challenging in the Alpujárride Complex where Fe-Mg carpholite is generally the only relic phase, in the form of needles inclusions in quartz lenses. To test this model and provide new constraints on the timing of the different Alpine metamorphic events recorded in the Alpujárride Complex (Azañón & Crespo-Blanc, 2000; Booth-Rea et al., 2005; Goffé et al., 1989), we undertook a search for new $^{40}Ar/^{39}Ar$ targets fulfilling this goal, that is, the best-preserved paragenesis for both H*P*-L*T* and L*P*-H*T* tectono-metamorphic events. We report new $^{40}Ar/^{39}Ar$ ages from white micas confirming (a) the occurrence of an Eocene H*P*/L*T* metamorphic event in post-Variscan Permian-Triassic micaschists displaying well-preserved H*P*/L*T* metamorphic parageneses associated with a syn-orogenic exhumation, and documenting (b) the effects of extensive overprinting at 20 Ma due to tectonic denudation and exhumation under H*T*/L*P* post-orogenic conditions.

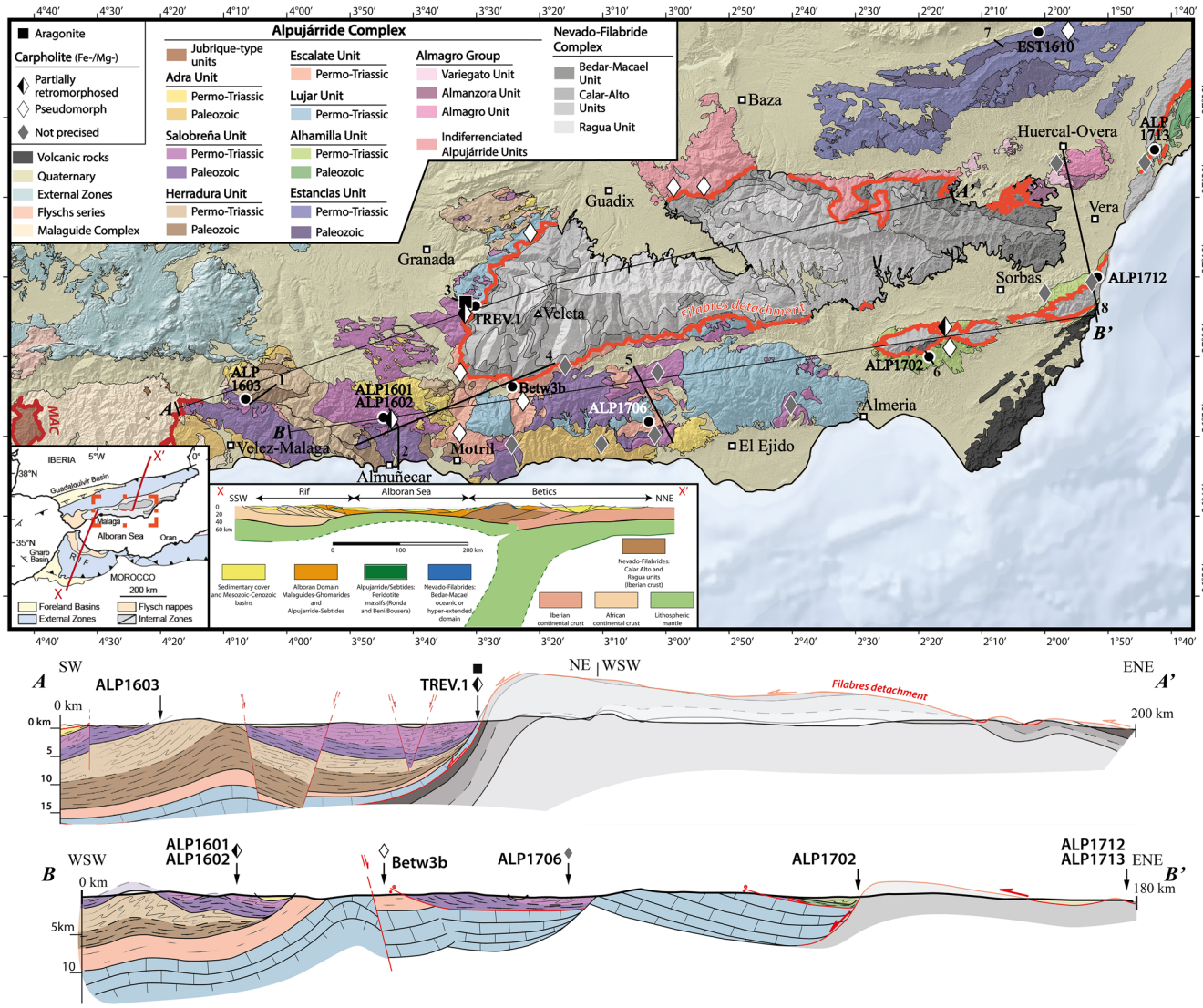

Figure 1. Geological and metamorphic map of the Betic Cordillera. Location of the Betic Cordillera belt within the Gibraltar arc. Detailed geological and tectono-metamorphic map of the Internal Zones of the Betic Cordillera, with the location of the studied area, and the location of the cross-sections. Regional cross-sections (A-A' and B-B') show the large-scale tectonic features of the study area. Position of the dated samples are projected, as well as the smaller-scale sections presented in Figures 5–12.

2. Geological Setting: Geodynamic Evolution of the Betic-Rif Orogen

The Betic-Rif Cordillera (western Mediterranean region) results from the Late Cretaceous-Eocene closure of the westernmost branch of the Neo-Tethys Ocean by subduction and collision of several crustal domains intercalated between Africa and Iberia. From the Oligocene to the Quaternary, slab dynamics including roll-back and tearing (Faccenna et al., 2004; Jolivet et al., 2008; Lonergan & White, 1997; Spakman & Wortel, 2004) formed a series of back-arc basins involving highly extended continental crust (e.g., the Alboran or the Aegean domains), volcanic material (Eastern Alboran basin), and juvenile oceanic crust (Tyrrhenian, Liguro-Provençal and Algerian basins; Faccenna et al., 2014; Jolivet et al., 2003; Menant et al., 2016; Michard et al., 2006; Prada et al., 2018). Later, compression took over after cessation of retreat of the Gibraltar subduction (Augier et al., 2013; Faccenna et al., 2004; Jolivet et al., 2006; Spakman et al., 2018). Accumulation of incremental tectono-metamorphic events is responsible for the highly arcuate finite shape of the belt, displaying a particularly high internal complexity (Augier, Agard et al., 2005; Booth-Rea et al., 2005; Esteban et al., 2011; de Jong, 1992; Li & Massonne, 2018;

López Sánchez-Vizcaíno et al., 2001; Monié et al., 1991, 1994; Platt et al., 2005, 2006, 2013; Sánchez-Rodríguez & Gebauer, 2000).

The northern branch of the arc (Betic Cordillera) is classically divided into unmetamorphosed External Zones and metamorphic Internal Zones (Egeler & Simon, 1969), separated by the internal-external boundary zone (IEBZ) where the Flyschs Complex is sandwiched (Figure 1; Durand-Delga, 1980; Vissers et al., 1995). A detailed exposition of the geology of the External Zones is provided by Vissers et al. (1995), Azañón and Crespo-Blanc (2000) or Platt et al. (2013).

The Internal Zones correspond to a stack of large-scale metamorphic complexes characterized by a poly-phased tectono-metamorphic record and are currently dominated by several sets of large-scale extensional shear zones (Agard et al., 2011; Augier, Booth-Rea et al., 2005; Augier, Jolivet, & Robin, 2005; Crespo-Blanc et al., 1994; Jabaloy et al., 1993; Martínez-Martínez et al., 2002; Platt, 1986; Vissers et al., 1995). Three main metamorphic complexes are usually recognized, from top to bottom (i.e., from the most external to the most internal): (a) the Malaguide, (b) the Alpujárride and (c) the Nevado-Filabride Complexes (Torres-Roldán, 1979), each separated by crustal-scale low-angle ductile, then brittle, extensional shear zones (Figure 1; Augier, Jolivet, & Robin, 2005; Martínez-Martínez et al., 2002; Platt et al., 2005, 2013; Vissers et al., 1995). Except for the Nevado-Filabride Complex, which is only observed on the Betic side, the other two complexes crop out on either side of the Alboran Sea, including the Rif. Our focus here is on the Alpujárride Complex for which we now provide the main geological, tectonic and metamorphic characteristics. The reader is referred to the Supporting Information S1 for a more detailed description of the Internal Zones.

2.1. The Alpujárride Complex

The Alpujárride Complex is a stack of several nappes including a Variscan basement and a Permian-Triassic metasedimentary cover of micaschists and marbles metamorphosed to various grades along different P/T ratios, and later dissected by low-angle normal faults (Azañón & Crespo-Blanc, 2000; Crespo-Blanc et al., 1994). This complex is affected by two main tectono-metamorphic events. The first one, coeval with subduction H*P*/L*T* metamorphic conditions (M1), is characterized by the development of a fabric (S1-L1) acquired during the first deformation phase (D1). Most Alpujárride Complex units indeed recorded H*P*/L*T* metamorphic imprint, as illustrated by the widespread occurrence of variably preserved carpholite and aragonite in veins associated with K white micas, pyrophyllite, chloritoid and chlorite (Azañón, 1994; Azañón & Crespo-Blanc, 2000; Booth-Rea et al., 2002, 2005; Figure 1). Peak-metamorphic conditions mostly cluster around a 10°C/km subduction gradient along which they reached variable H*P*/L*T* conditions at ca. 10 ± 2 kbar and 400 ± 100°C (Figure 2; Azañón & Crespo-Blanc, 2000; Platt et al., 2013). The second deformation stage (D2) is associated to an important extensional event, related to the polyphased exhumation of the complex during both syn- and late-orogenic stages, leading to the development of the main regional gently dipping planar-linear fabric (S2-L2) across the whole metamorphic complex (Figure 2; Azañón, 1994; Azañón & Crespo-Blanc, 2000; Azañón et al., 1997; Booth-Rea et al., 2005). During D2, the S1 fabrics is pervasively crenulated while the M1 H*P*/L*T* metamorphic paragenesis appear only and often partially preserved within veins (Figure 2). Metamorphic conditions (M2) are characterized by low pressures around 3–4 kbar for similar ca. 400°C temperatures (Azañón et al., 1993, 1997, 1998; Azañón & Crespo-Blanc, 2000; Bakker et al., 1989; Monié et al., 1994). Exhumation to near surface conditions was almost complete when a third deformation stage (D3) occurred. This event, associated to a renewal of crustal contraction, is characterized by new nappe stacking event and large-scale folding (Azañón & Crespo-Blanc, 2000). Finally, the fourth stage (D4) corresponds to the segmentation of the exhumed metamorphic rocks by the extensive development of regional-scale high-angle normal faults affecting the whole complex (Azañón & Crespo-Blanc, 2000; Tubía et al., 1992).

2.2. Alpine *P-T* Evolution of the Alpujárride Complex

One puzzling feature of the Alpujárride Complex is the metamorphic contrast between the western and central-eastern parts. The central and eastern Alpujárride Complex units show widespread H*P*-L*T* relics that are completely lacking in the western part, except for the retrogressed Ojén eclogites (Azañón & Crespo-Blanc, 2000; Azañón et al., 1992, 1997; Bakker et al., 1989; Booth-Rea et al., 2002; Goffé et al., 1989; Tubía & Gil Ibarguchi, 1991).

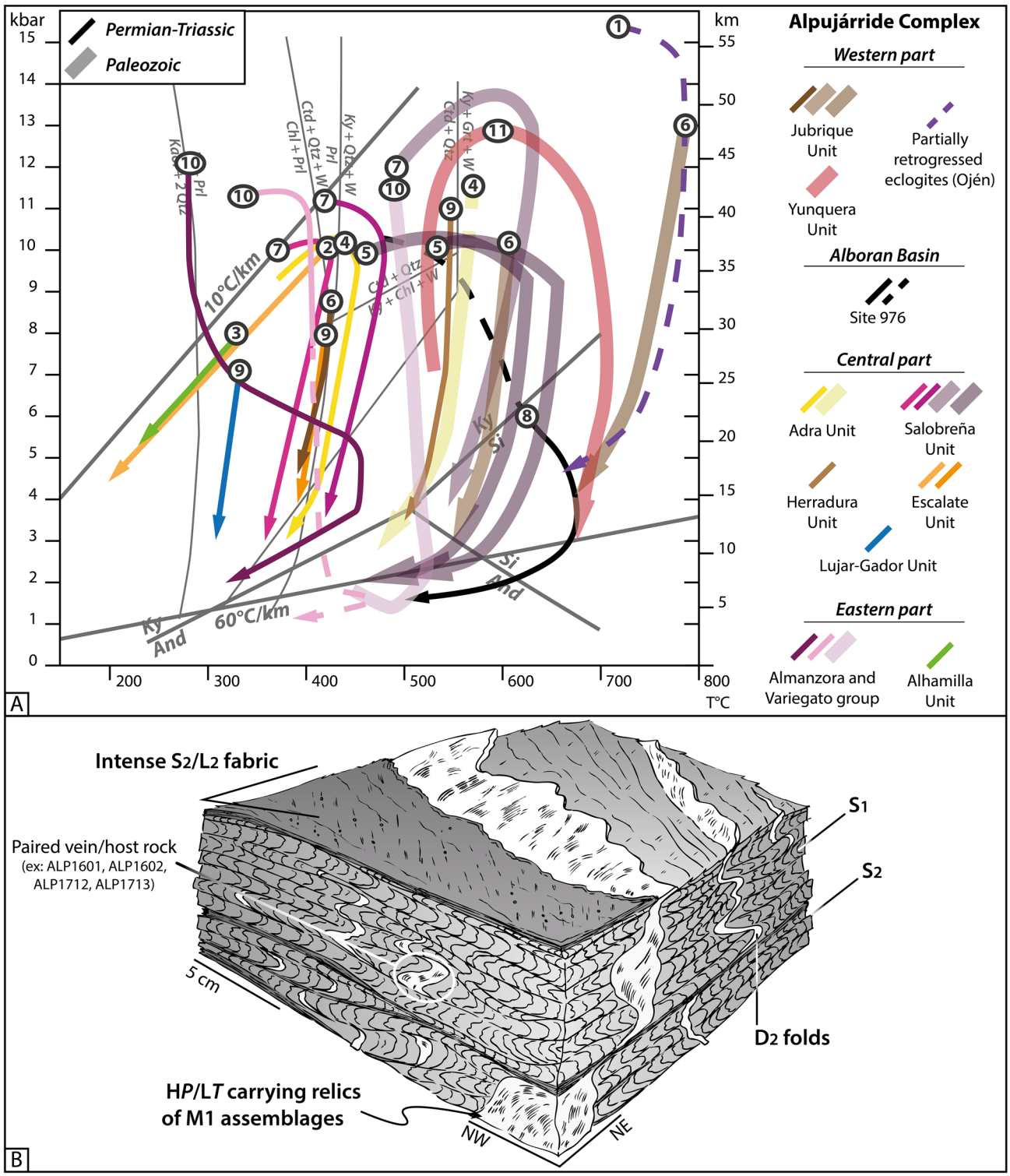
kbar
km
T°C
Permian-Triassic
Paleozoic
10°C/km
60°C/km
Ky And
Si And
Alpujárride Complex
Western part
Jubrique Unit
Partially retrogressed eclogites (Ojén)
Yunquera Unit
Alboran Basin
Site 976
Central part
Adra Unit
Salobreña Unit
Herradura Unit
Escalate Unit
Lujar-Gador Unit
Eastern part
Almanzora and Variegato group
Alhamilla Unit
A
Intense S2/L2 fabric
Paired vein/host rock
(ex: ALP1601, ALP1602, ALP1712, ALP1713)
S1
S2
5 cm
D2 folds
HP/LT carrying relics of M1 assemblages
NW
NE
B

Figure 2.

Mineralogical assemblages related to this H*P*/L*T* event, M1, include carpholite, kyanite, chloritoid and aragonite, which developed during the subduction of continental slivers, particularly within the Permian-Triassic metasediments (Azañón & Crespo-Blanc, 2000; Azañón et al., 1992, 1997, 1998; Azañón & Goffé, 1997a, 1997b; Balanyá et al., 1997; Booth-Rea et al., 2002; de Jong, 1991; Goffé et al., 1989; Jolivet et al., 2003). In contrast, the Paleozoic dark metasediments displays mostly high-temperature parageneses with garnet, staurolite, biotite, andalusite and locally sillimanite (Figure 2; Azañón & Crespo-Blanc, 2000; Azañón et al., 1992, 1997; Azañón & Goffé, 1997a, 1997b; Booth-Rea et al., 2005; Goffé et al., 1989; Jolivet et al., 2003). Similar observations can be made in the Paleozoic dark metasediments of the western part of the Alpujárride Complex and the Permian-Triassic metasediments. Both either lack evidence for H*P*/L*T* metamorphism, or display only H*P*-mineral relics, with a dominant H*T*-L*P* metamorphic record (Acosta-Vigil et al., 2016, 2014; Balanyá et al., 1997; Barich et al., 2014; Bartoli et al., 2013, 2016; Esteban et al., 2005, 2008; Massonne, 2014; Ruiz-Cruz & Sanz de, 2014; Tubía et al., 1997). The Permian-Triassic metasediments from the central and eastern Alpujárride units, which have not recorded any pre-Alpine metamorphic event, show peak-pressure conditions between 10 and 12 kbar at temperatures mostly ranging from 300°C to 450°C, and only locally 550°C in the Herradura unit (Figure 2; Azañón et al., 1998; Azañón & Goffé, 1997a, 1997b; Booth-Rea et al., 2005). Some tectonic units recorded lower pressure conditions, mostly around 7–8 kbar, at temperatures between ∼280°C and ∼400°C (Figure 2; Azañón et al., 1992, 1998; Azañón & Goffé, 1997a, 1997b).

Two main *P-T* evolutions can be distinguished with, (a) a retrograde path along a cold gradient around 10°C/km, typical of syn-orogenic exhumation in the subduction complex, and (b) a nearly isothermal decompression characteristic of post-orogenic exhumation (Figure 2). The first type of retrograde *P/T* evolution is characterized by the good preservation of H*P*/L*T* metamorphic assemblages (involving the Escalate and Alhamilla units only; see Figure 1; Azañón et al., 1992, 1997, 1998; Azañón & Goffé, 1997a, 1997b; Goffé et al., 1989, 1996). The second type of retrograde *P/T* evolution occurred at amphibolite-facies to upper-greenschist-facies, until pressure conditions near ∼3–4 kbar and temperature conditions between 300 and 420°C, or 500°C for the Herradura unit (Figure 2; Azañón & Crespo-Blanc, 2000; Azañón et al., 1993, 1997, 1998; Bakker et al., 1989; Monié et al., 1994). These led to extensive overprinting of H*P*/L*T* parageneses, locally leaving only scattered relics or pseudomorphs (Azañón et al., 1992, 1998; Azañón & Goffé, 1997a, 1997b; Booth-Rea et al., 2005; Goffé et al., 1989, 1996).

2.3. Previous Geochronology for Alpine Evolution of the Alpujárride Complex

Available ages for M1, the H*P*/L*T* metamorphic event related to the first deformation phase (D1) are scarce and correspond only to $^{40}Ar/^{39}Ar$ on barroisite and white micas. Age data range between Eocene and Oligocene, that is, from ∼48 Ma (no spectra shown), to less than 23 Ma (Figure 3; Monié et al., 1991; Platt et al., 2005). The D2 event, responsible for a strong metamorphic overprint (M2), has also been dated using $^{40}Ar/^{39}Ar$ on white micas yielding early Miocene ages, mostly clustered around the Aquitanian-Burdigalian boundary around 20 Ma (Figure 3; Monié et al., 1991, 1994; Platt et al., 2005). Many other ages (obtained using both $^{40}Ar/^{39}Ar$ and U/Pb methods; see Figure 3) provided in other studies discussing the succession of tectono-metamorphic events, especially those post-dating the D1 phase and the M1 conditions, were obtained on pre-Alpine metamorphic rocks potentially affected by inherited, mixed, ages (Esteban et al., 2011; Frasca et al., 2017; Loomis, 1975; Platt et al., 2003, 2005; Platt & Whitehouse, 1999; Priem et al., 1979; Sánchez-Rodríguez & Gebauer, 2000; Sosson et al., 1998; Whitehouse & Platt, 2003; Zeck & Williams, 2001). The need to work on fresh samples obviating such shortcomings appears thus essential to clear up this issue, as we next discuss.

Figure 2. Synthesis of *P-T* paths and main tectono-metamorphic events in the Alpujárride Complex and sampling strategy. (a) Synthesis of retrograde *P-T* paths recorded by each unit from the Alpujárride Complex, with the distinction between the Paleozoic and Permian-Triassic lithostratigraphic units (large and pastel lines vs. thin and dark lines). Data are from (1) Tubía and Gil Ibarguchi (1991); (2) Azañón et al. (1992); (3) Goffé et al. (1994); (4) Azañón et al. (1995); (5) García-Casco and Torres-Roldán (1996); (6) Balanyá et al. (1997); (7) Azañón et al. (1998); (8) Soto and Platt (1999); (9) Azañón and Crespo-Blanc (2000); (10) Booth-Rea et al. (2005) and (11) Esteban et al. (2005). (b) Synthetic 3D sketch derived from field observation and illustrating the two main metamorphic events observed in the Alpujárride Complex, that is, the high-pressure/low-temperature (H*P*/L*T*) metamorphic event (M1) and the H*T*/L*P* metamorphism (M2). The almost transposition of the S1 by the S2 is highlighted by the penetrative foliation developed during the D2 phase under warmer temperature conditions due to the post-orogenic extensional exhumation, allowing the folding and the partial overprint of the H*P*/L*T* markers. Also shown are relationships between quartz-veins and the host micaschist parts which can be typically observed for paired samples: ALP1601, ALP1602 and ALP1712/ALP1713.

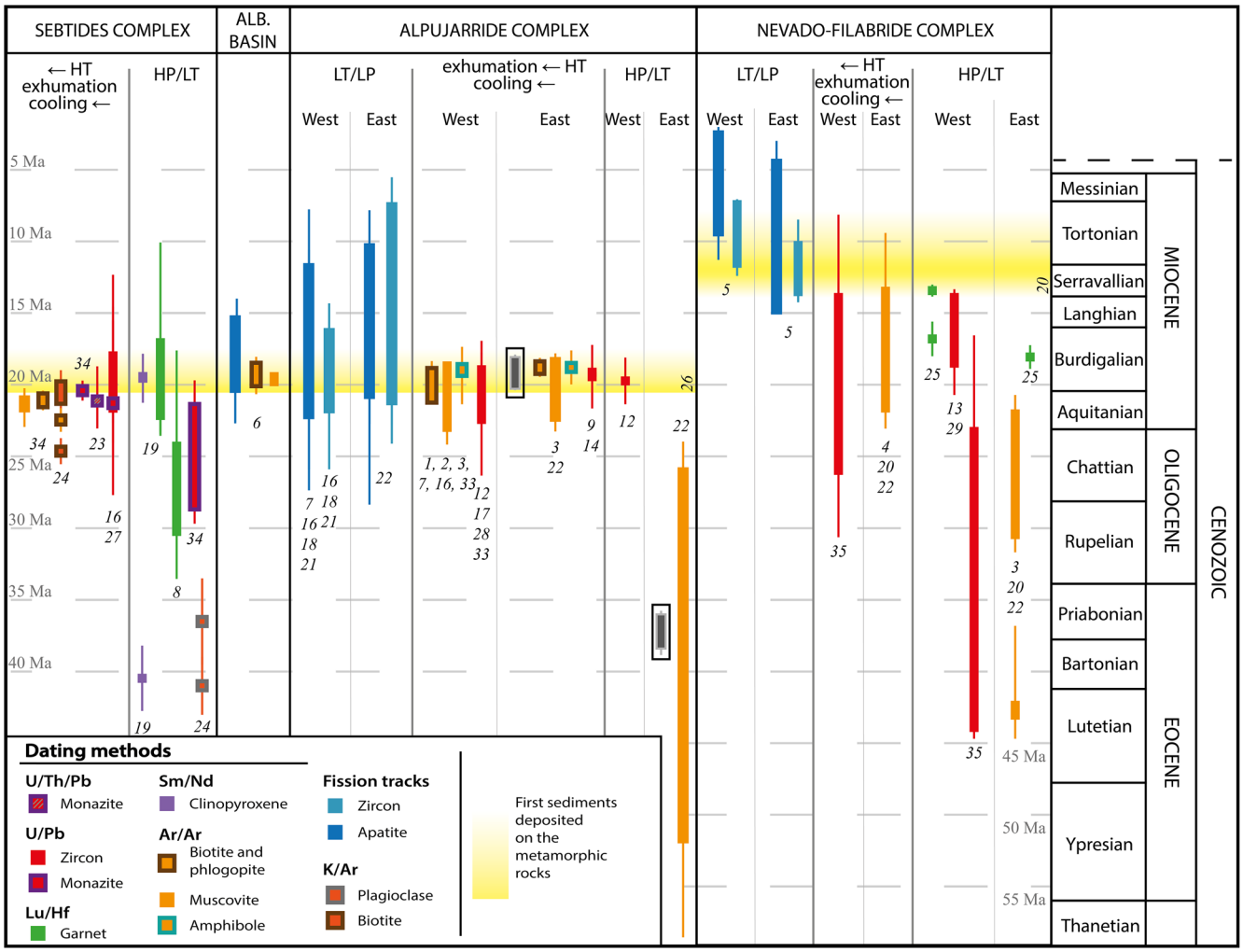

Figure 3. Synthesis of the available geochronological data for the Internal Zones of the Betic-Rif Cordillera. Summarize of the available tectono-metamorphic dating in the studied area, that is, the Internal Zones of the Betic-Rif Cordillera. Results from the Sebtide Complex (the Rifan twin of the Alpujárride Complex) are given for comparison. Black boxes are dating from this study. Numbers refer to the references as follow: (1) Loomis (1975); (2) Priem et al. (1979); (3) Monié et al. (1991, 1994); (4) de Jong (1992); (5) Johnson et al. (1997); (6) Platt et al. (1998); (7) Sosson et al. (1998); (8) Blichert-Toft (1999); (9) Platt and Whitehouse (1999); (10) Zeck and Whitehouse (1999); (11) Montel et al. (2000); (12) Sánchez-Rodríguez and Gebauer (2000); (13) López Sánchez-Vizcaíno et al. (2001); (14) Zeck and Williams (2001); (15) Zeck and Whitehouse (2002); (16) Platt et al. (2003); (17) Whitehouse and Platt (2003); (18) Esteban et al. (2004); (19) Pearson and Nowell (2004); (20) Augier, Agard et al. (2005); Augier, Booth-Rea et al. (2005); (21) Esteban et al. (2005); (22) Platt et al. (2005); (23) Janots et al. (2006); (24) Michard et al. (2006); (25) Platt et al. (2006); (26) Serrano et al. (2006); (27) Rossetti et al. (2010); (28) Esteban et al. (2011); (29) Gómez-Pugnaire et al. (2012); (30) Acosta-Vigil et al. (2014); (31) Massonne (2014); (32) Ruiz-Cruz and Sanz de Galdeano (2014); (33) Frasca et al. (2017); (34) Homonnay et al. (2018); (35) Li and Massonne (2018).

3. Sampling Strategy and Sample Description

3.1. Sampling Strategy

The main question motivating this work is whether an Eocene M1, the H*P*/L*T* event, affected the whole Alpujárride subduction complex and, if so, what is the timing of this event and the subsequent H*T*/L*P* overprint that can be deduced from $^{40}Ar/^{39}Ar$ dating on white micas (Monié et al., 1991; Platt et al., 2005). Despite the late M2 H*T* overprint, early diagnostic H*P*/L*T* parageneses are locally preserved in the central and eastern parts of the complex that did not experience temperatures exceeding 350–400°C (Figures 2–4; Azañón, 1994; Booth-Rea et al., 2005; Goffé et al., 1989, 1996). Such rare H*P*/L*T* relics occur associated with H*P*/L*T* metamorphic assemblages including aragonite, Fe-Mg-carpholite, saliotite and sudoite carried by the D1 (S1/L1) fabrics and the veins (Azañón, 1992; Azañón et al., 1997; Goffé et al., 1989, 1994, 1996, Figures 2 and 4).

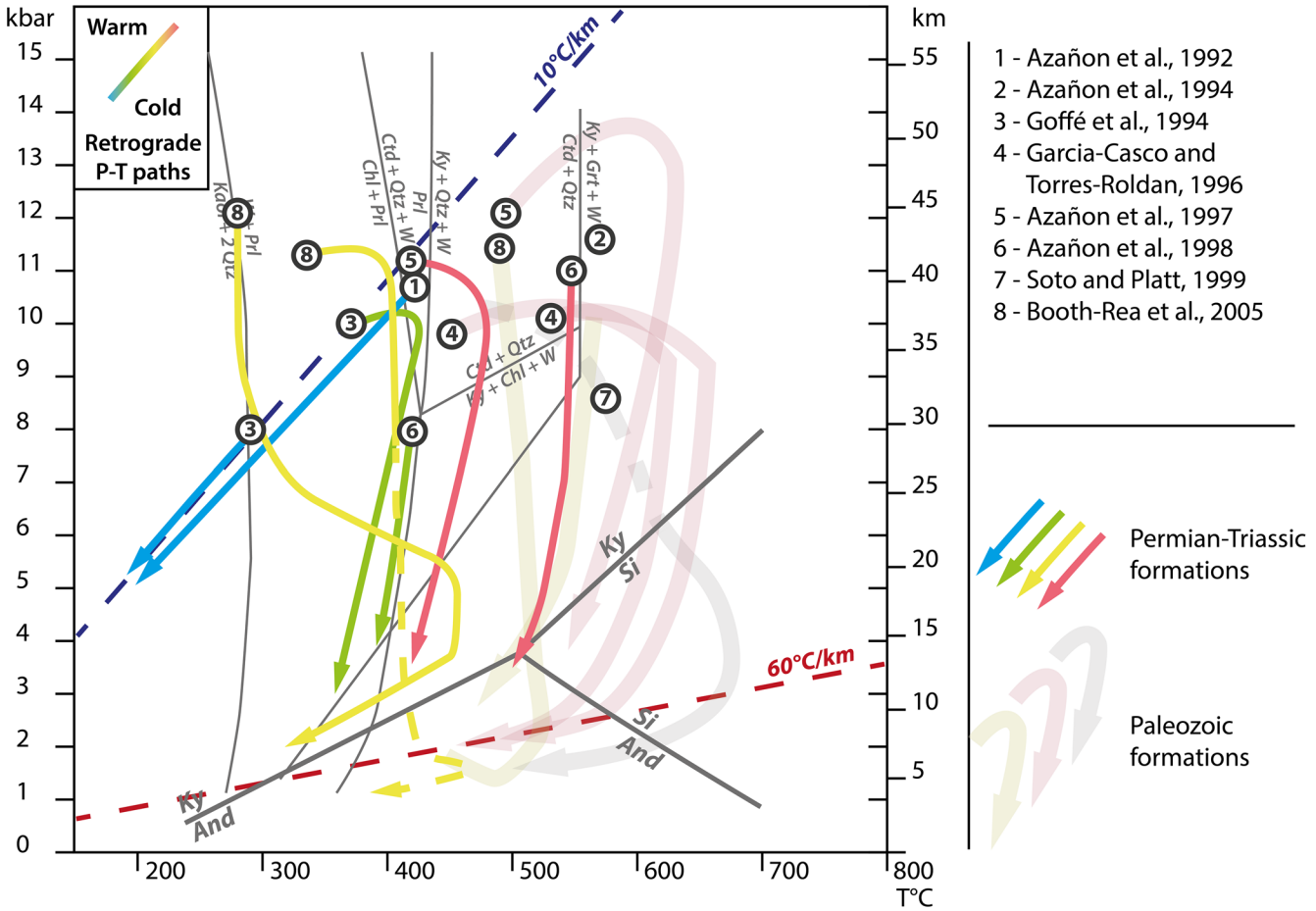

Figure 4. Diversity of the retrograde *P-T* paths for the Alpujárride tectonics units dated in this study. Units were distinguished and ordered upon the type of their retrograde *P-T* paths, including cooling, sub-isothermal decompression or heating. Sampling focused on the Permian-Triassic metasedimentary succession of the Alpujárride Complex; *P-T* paths of the Paleozoic lithostratigraphic formations are given for comparison.

To achieve this goal, 10 samples were selected based on the spatial distribution of such index mineral associations and by applying the following guidelines (see location map in Figure 1). First, the sampling was primarily focused on Permian-Triassic formations to avoid possible complications due to a Variscan isotopic inheritance (Figures 2 and 4; Booth-Rea et al., 2005; Goffé et al., 1989; Puga et al., 2011; Tubía & Gil Ibarguchi, 1991). The only exception is sample ALP1702 from the Paleozoic graphitic schists of the Sierra Alhamilla where kyanite veins are clearly associated with the Alpine M1 event. Besides, the Permian-Triassic formations above never experienced temperatures over 300°C (Figures 2 and 4; Goffé et al., 1989, 1994, 1996) and thus escaped the late Miocene M2 metamorphic event, suggesting that the whole sequence from the Paleozoic graphitic schists to the Triassic carbonates also escaped the M2 event. Next, to check this inference, different structural levels were sampled through a same unit (Salobreña unit) where *P-T* estimates are available (Azañón, 1994; Azañón et al., 1997; Booth-Rea et al., 2002, 2005; Goffé et al., 1989, 1996; Platt et al., 2005), from the top of the sequence, where Permian-Triassic series record an Alpine maximum temperature around 430°C, to the base where the Paleozoic metasediments have possibly recorded the late Oligo-Miocene thermal event. Finally, we sampled schists and associated veins with preserved M1 mineralogical assemblages. The veins are undeformed but found included in host rocks affected by ductile deformation. Both the host rocks and the veins were sampled to evaluate the mica isotopic response according to textural setting (Figure 2b).

It is worth to mentioning that samples were selected from the same outcrops previously used for *P-T* calibration in Azañón (1992), Azañón et al. (1997, 1998), Azañón and Goffé (1997a, 1997b), Azañón and Crespo-Blanc (2000) and Platt et al. (2005).

3.2. Samples Description

Sample locations are shown on the geological map of Figure 1 and their specific setting (cross-sections) is described in the following figures (Table 1, Figures 1 and 3). All samples were taken from areas where *P-T* estimates are available (Azañón et al., 1992, 1997, 1998; Azañón & Goffé, 1997a, 1997b; Booth-Rea et al., 2005; Goffé et al., 1989, 1996).

ALP1603 consists of a meta-quartzite of the Herradura unit, showing a garnet-kyanite-plagioclase assemblage recording peak-pressure conditions of 11 ± 1 kbar and peak-temperature conditions around 580 ± 40°C (Figures 1, 5a and 5b; Azañón et al., 1997). Samples ALP1601 and ALP1602 were collected in the lower part of the metapelites of Salobreña Unit, containing Fe-Mg-carpholite + kyanite or chloritoid + kyanite + chlorite assemblages in veins (Table 1, Figures 1 and 6a–6c), yielding a pressure of 10 ± 2 kbar and a temperature of 450 ± 30°C (Table 1, Figures 1, 2 and 4). Pyrophyllite-bearing micaschist TREV.1 belongs to the upper part of the Salobreña unit, very close to the major tectonic contact with the Nevado-Filabride Complex, at Trevenque Pass (Figures 1 and 7a). Rocks of this unit are characterized by Fe-Mg-carpholite + chlorite preserved in quartz-veins, with occasional kyanite and aragonite (Table 1, Figure 1). Estimated metamorphic conditions are 9 ± 2 kbar and 420 ± 30°C (Azañón et al., 1992) and the good preservation of the M1 minerals, that is, carpholite and aragonite, testifies for the absence of significant M2 metamorphic overprint (Table 1 and Figures 2 and 4). Betw3b is a light-colored carpholite + pyrophyllite + quartz schist of the Escalate unit, close to the tectonic contact with the Nevado-Filabride Complex and comprising metapelites, metacarbonates and metaquartzites (Figures 1 and 8a). Occasional chloritoid is present along with fibers of Fe- or Mg-carpholite (Azañón et al., 1992; Azañón & Goffé, 1997a, 1997b; Goffé et al., 1989). Metamorphic peak-pressure conditions are estimated around 7–9 kbar and peak-temperature conditions between 380 and 430°C. ALP1706 is a low-grade phyllite from Escalate unit (Rio Grande area) showing the mineralogical assemblage white mica + paragonite + chlorite + albite with local carpholite relics, which yields peak-pressure conditions of 7.5 ± 1.0 kbar for temperatures <420°C (Figures 1 and 9; Azañón et al., 1997; Platt et al., 2005). Sample ALP1702 was selected in the pre-Permian Paleozoic graphitic metasediments exposed in the southern parts of the Sierra Alhamilla displaying spectacular kyanite-bearing quartz-veins associated with white micas formed during the Alpine retrograde metamorphic event (Table 1, Figures 1, 10a–10c). The host rock of these veins is a medium-grade micaschist characterized by garnet + staurolite + kyanite + muscovite + biotite + rutile formed/equilibrated at around 10 kbar and 540–600°C. These metamorphic conditions are probably related to the Variscan orogeny. The veins only recorded the Alpine retrograde metamorphic event with an estimated peak pressure around 8 kbar with an associated temperature higher than 380°C (Table 1, Figures 2 and 4; Azañón & Goffé, 1997a, 1997b; Goffé et al., 1994). ALP1712 was sampled in the Triassic phyllites of Sierra Cabrera, and ALP1713 in the Triassic phyllites of Sierra Almagrera (Figures 1 and 11). These last two samples belong to the Variegato unit located close to the contact with the Nevado-Filabride Complex. They are Mg-carpholite + pyrophyllite chlorite-schists with pyrophyllite quartz-veins, giving metamorphic peak conditions of 9 ± 1 kbar and 380 ± 30°C (Booth-Rea et al., 2005). EST1610 was collected in the Permian meta-conglomerate cropping out in the northern parts of the Sierra de las Estancias, around 7 km east of Vélez-Rubio (Figures 1 and 12). These metamorphic rocks contain muscovite, chlorite and locally chloritoid ± kyanite ± carpholite relics that returned pressure estimates of ∼7 kbar for temperature close to 450°C (Platt et al., 2005).

4. Texture, Microstructure, and Mineral Composition

Macroscopic and microscopic observations and chemical compositions of the $^{40}Ar/^{39}Ar$ samples are described below in connection with their Alpine tectono-metamorphic record (Figures 5–12).

ALP1603 (Figure 5) corresponds to a garnet-kyanite quartz-rich quartzite displaying a strong D2 (S2/L2) fabrics. Large white mica grains reaching 2–3 mm are mostly secant to the main foliation (S2) and grown in pressure shadows around deformed garnet or kyanite or in between fragments of stretched and truncated kyanite parallel to L2 (Figures 5c and 5d). Quartz locally shows an important grain-size reduction. White micas display slightly scattered compositions, with some Fe-rich to Fe-poor core-to-rim variations (Figure 5e). In addition, X_{Mg} shows a wide dispersion from c. 0.14 to c. 0.55, while the Si^{4+} content is comprised between c. 3.0 and c. 3.22 (Figure 5f). ALP1601 and ALP1602 samples (Figure 6), collected a few meters apart, are associated to metamorphic veins hosted in deformed chlorite-bearing light-gray micaschists (ALP1601h, Figures 6b and 6c) as described

Tectonics
10.1029/2021TC006889

Table 1
Summary of Samples From the Central and Eastern Alpujárride Complex, With the Lithology, the Mineral Assemblages, the P-T Conditions Associated, the Unit and the Localities Where Sampling Have Been Operated, Associated to the Coordinates and the Step-Heating Method Used, That is, Single-Grain (Sg), Mica Population (Pop) or Mica Aggregate (Agg), and the White Mica $^{40}Ar/^{39}Ar$ Results, That is, the Total Apparent Age Obtained and the Associated "Plateau Age"

Sample	Lithology	Carpholite observed or described	Mineral assemblages of the unit	*P-T* conditions	Unit	Localities	Lat	Long	Method	TGA (Ma)	"Plateau age" (Ma)
ALP1601h	Permo-triassic cld-ky meta-pelitic schists		Mg-cph + ky + cld + chl	10 ± 2 kbar	Salobreña	Otivar	36.836806°	−3.704833°	agg	30.2 ± 0.3	-
										29.8 ± 0.3	-
ALP1601v	qz-vein of the Permo-triassic cld-ky schists	x			Salobreña				pop	20.3 ± 0.2	-
ALP1602h	Permo-triassic cld-ky meta-pelitic schists			430 ± 50°C	Salobreña	Otivar	36.833500°	−3.706278°	agg	21.2 ± 0.2	-
										21.9 ± 0.2	-
ALP1602v	qz-vein of the Permo-triassic cld-ky schists	x			Salobreña				pop	19.6 ± 0.2	-
ALP1603	Permo-triassic meta-quartzite		grt + ky + pl	11 ± 1 kbar 580 ± 40°C	Herradura	Canillas de Aceituno	36.869167°	−4.065639°	pop	20.4 ± 0.2	-
ALP1702v	ky-quartz-vein in Paleozoic garnet graphitic schist		ky + qz + micas	8–12 kbar 300–480°C	Alhamilla	Nijar	36.961210°	−2.295880°	sg	19.5 ± 0.2	19.52 ± 0.04
										15.7 ± 0.4	-
ALP1706	low-grade Permo-triassic phyllite		phg + par + chl + alb	7.5 ± 1 kbar <420°C	Escalate	El Rio Grande (Berja)	36.827600°	−3.021490°	agg	41.6 ± 0.5	-
										52.7 ± 0.6	-
ALP1712h	Triassic phyllite		chl + Mg-cph + pyr + qz	9 ± 1 kbar	Variegato	Mojacar	37.122220°	−1.853620°	agg	no argon content	
ALP1712v	vein in Triassic phyllite	x			Variegato				pop	17.7 ± 0.3	18.1 ± 0.2
ALPA1713h	Triassic phyllite			380 ± 30°C	Variegato	La Galeria - Pilar de Jaravia (Pulpi)	37.385880°	−1.699500°	agg	22.3 ± 0.3	-
										20.4 ± 0.3	-
ALP1713v	vein in Triassic phyllite	x			Variegato				pop	no argon content	
EST1610	Permian meta-conglomerate		chl + ms + cld + ky/car	~7 kbar ~450°C	Estancias	Vélez-Rubio	37.631411°	−2.004945°	agg	22.5 ± 0.3	-
										24.1 ± 0.3	-
TREV.1	Permo-triassic chl pyrophyllite with qz veins	x	cph + chl + qz	9 ± 2 kbar 420 ± 30°C	Salobreña	Trevenque Pass (Granada)	37.067278°	−3.474694°	pop	37.9 ± 0.4	-
										38.2 ± 0.4	-
Betw3b	Light-colored schists with alternation of meta-carbonates and quartzites	x	Fe-Mg-cph + prl + chl + qz	9 kbar 380–430°C	Escalate	Orgiva	36.905022°	−3.371428°	agg	18.9 ± 0.2	18.9 ± 0.03

Note. Mineral assemblages and the associated *P-T* conditions are after Azañón et al. (1992, 1995, 1997, 1998); Goffé et al. (1994); Azañón and Goffé (1997a, 1997b); Booth-Rea et al. (2002, 2005); Platt et al. (2005).

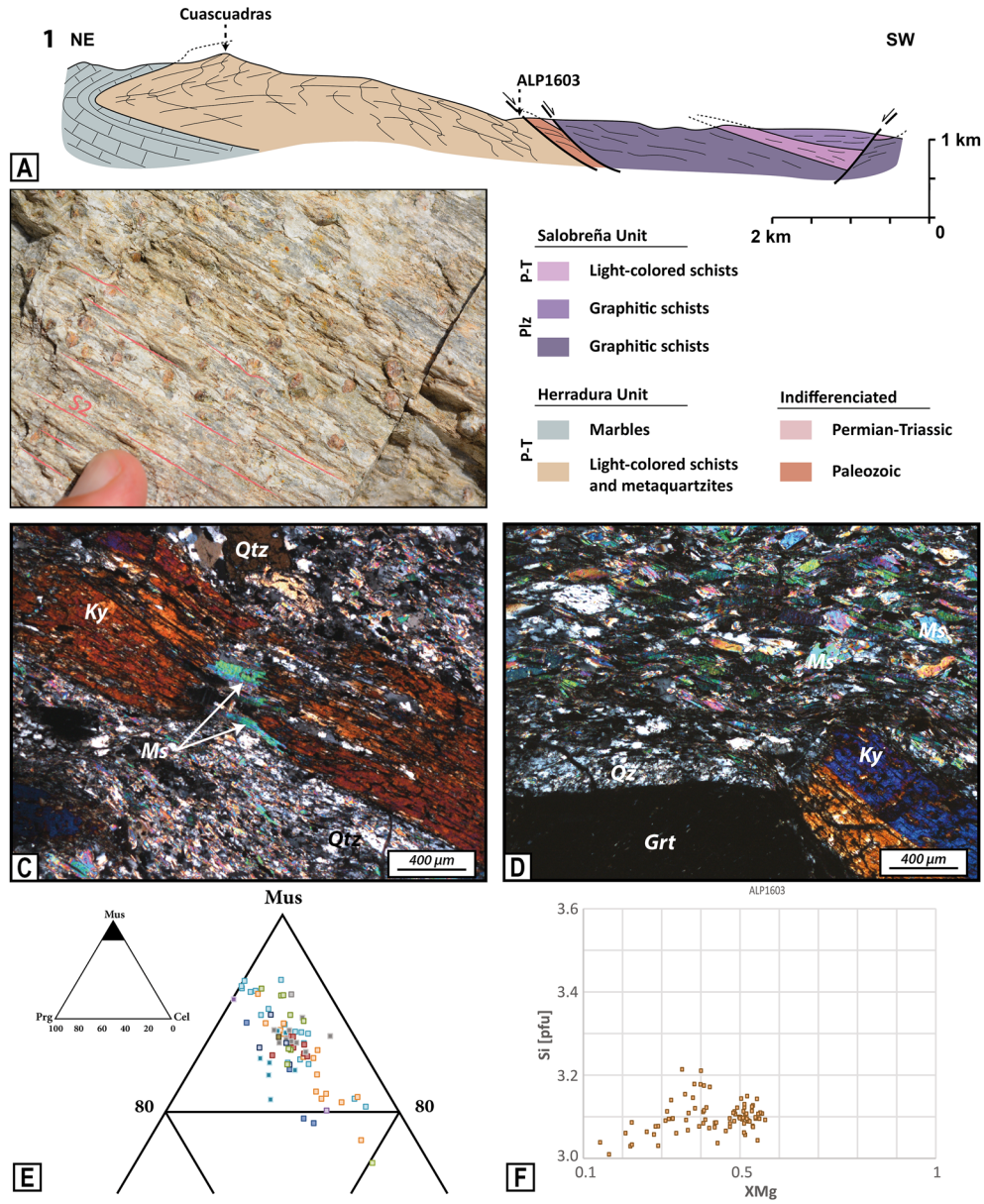

Figure 5. Summary of the structure, petrography and chemical composition for the sample ALP1603. (a) Geological and tectonic cross-section of the sampled area and location of the sample, modified after Alonso-Chaves and Orozco (2007). (b) Detailed view of the outcrop where the ALP1603 sample was selected. (c and d) Thin-section observations of the dated sample (polarized light). (e) Ternary composition plot for white micas. (f) Variation of X_{Mg} versus Si^{IV} contents in white micas.

in Figure 2. These latter are mainly composed of fine-grained white micas, quartz and chlorite defining a very fine-grained S1 foliation mainly marked by the alignment of white micas deformed by D2 microfolds. Slightly coarser grained white micas occur in cleavage domains where S2 is best expressed (Figure 6d). In contrast, the metamorphic vein (i.e., ALP1601v) is undeformed and coarse-grained with kyanite + white mica + calcite (Figure 6e). White mica composition shows large differences between the host rock and the vein, with a greater paragonite content in the host rock and higher muscovite content in the vein (Table 2 and Figure 6f). X_{Mg} is also variable with values ranging from 0.25 and 0.5 with a clustering around 0.3 (host rock, unfilled orange squares Figure 6g), and from 0.27 to 0.43 with a strong clustering between 0.32 and 0.37 (quartz vein, filled orange squares Figure 6g). White mica Si content is comprised between 3.0 and 3.12 in the host and between 3.02 and 3.23 in the veins (respectively unfilled and filled orange squares Figure 6g). Micaschist TREV.1 (Figure 7)

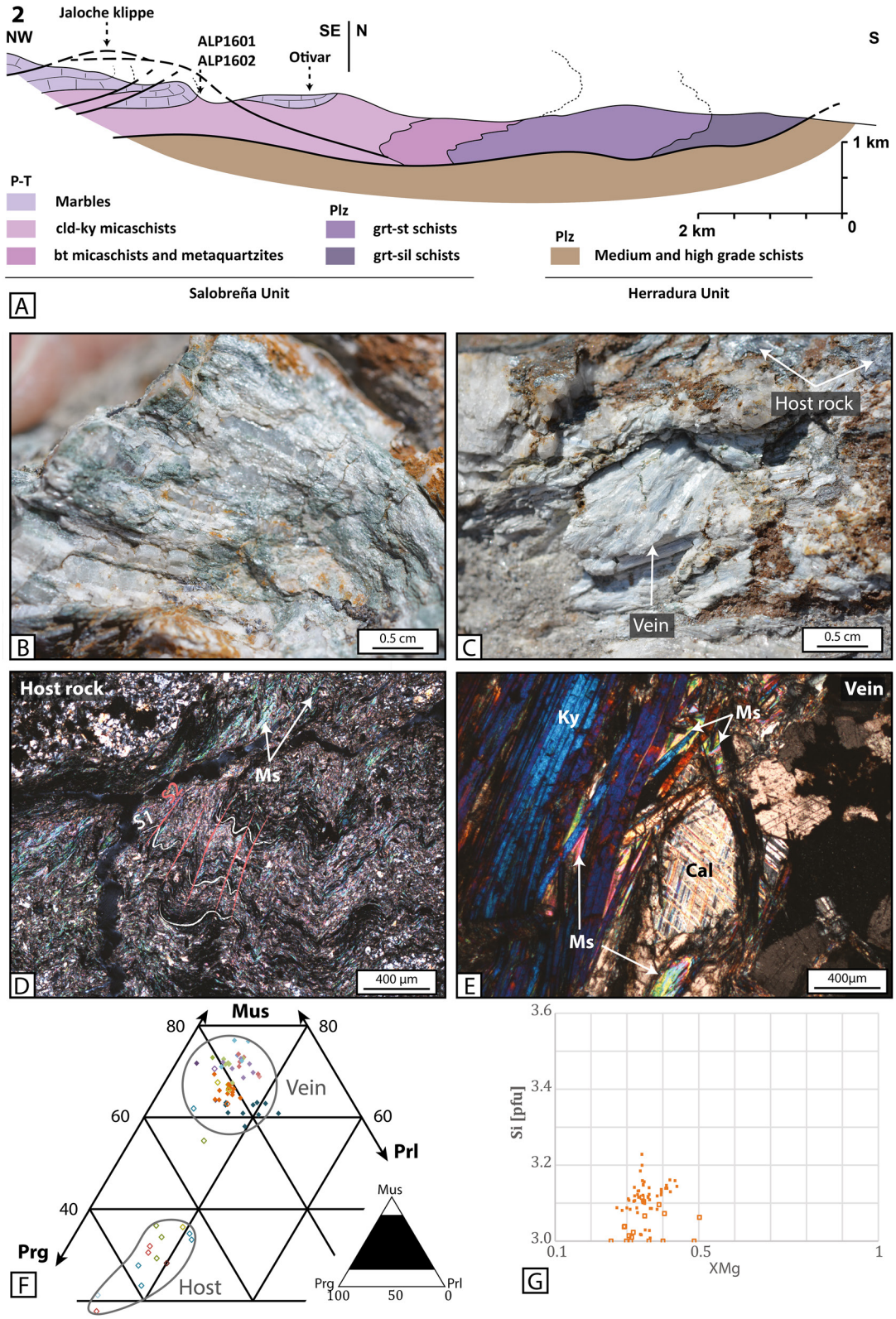

Figure 6. Summary of the structure, petrography and chemical composition for the samples ALP1601 and ALP1602. (a) Geological and tectonic cross-section of the sampled area and location of the samples, modified after Azañón et al. (1998). (b and c) Detailed view of the outcrop where the ALP1601 and ALP1602 samples were selected. (d and e) Thin-section observations of the dated samples (polarized light) including (d) the host rock part and (e) the vein part. (f) Ternary composition plot for white micas. (G) Variation of X_{Mg} versus Si^{IV} contents in white micas.

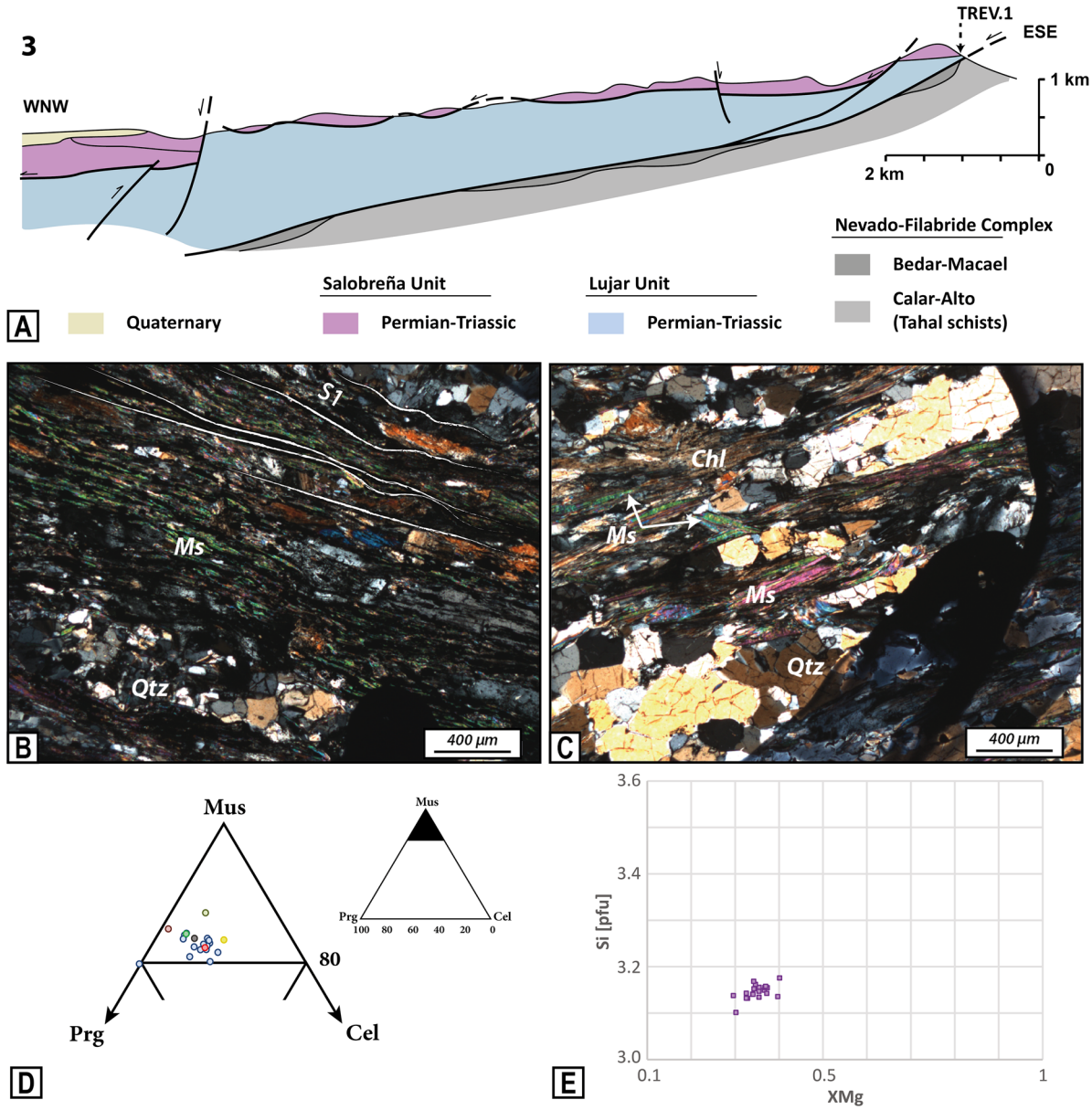

Figure 7. Summary of the structure, petrography and chemical composition for the sample TREV.1. (a) Geological and tectonic cross-section of the sampled area and location of the TREV.1 sample, modified after Sanz de Galdeano and Lopez Garrido (1999). (b and c) Thin-section observations of the dated sample (polarized light). (d) Ternary composition plot for white micas. (e) Variation of X_{Mg} versus Si^{IV} contents in white micas.

contains Fe-Mg carpholite, quartz, white micas and chlorite, associated with a single well-developed S1 planar fabric. White micas appear undeformed and are sometimes oblique to the main foliation (S1, Figures 7b and 7c). In addition, chlorite shows a weak deformation while quartz grains do not seem deformed (Figure 7c). White mica composition is homogeneous with relatively constant X_{Mg} and Si content from ca. 0.29 to ca. 0.40 and ca. 3.1 and ca. 3.18, respectively (Table 2 and Figures 7d and 7e). Betw3b (Figure 8) is a light-colored micaschist composed of alternating quartz-rich and mica-rich layers. Mineralogy includes quartz, biotite, kyanite and white micas and characterized by a locally well-developed S1 foliation and a locally heterogeneous quartz grain-size (Figures 8b and 8c). Mica-rich layers show spaced microfolds and the weak development of S2 carrying white mica and biotite (Figure 8c). Micas also occur as post-tectonic porphyroblasts indicating that they grew at least at the end of the D2 deformation episode (Figure 8c). The composition of white mica falls dominantly close to the muscovite endmember (Figure 8d). The observed X_{Mg} shows variations from ca. 0.31 to ca. 0.55 and for the Si content, which is comprised between ca. 3.10 and ca. 3.19 (Figure 8e). ALP1706 (Figure 9) is an extremely

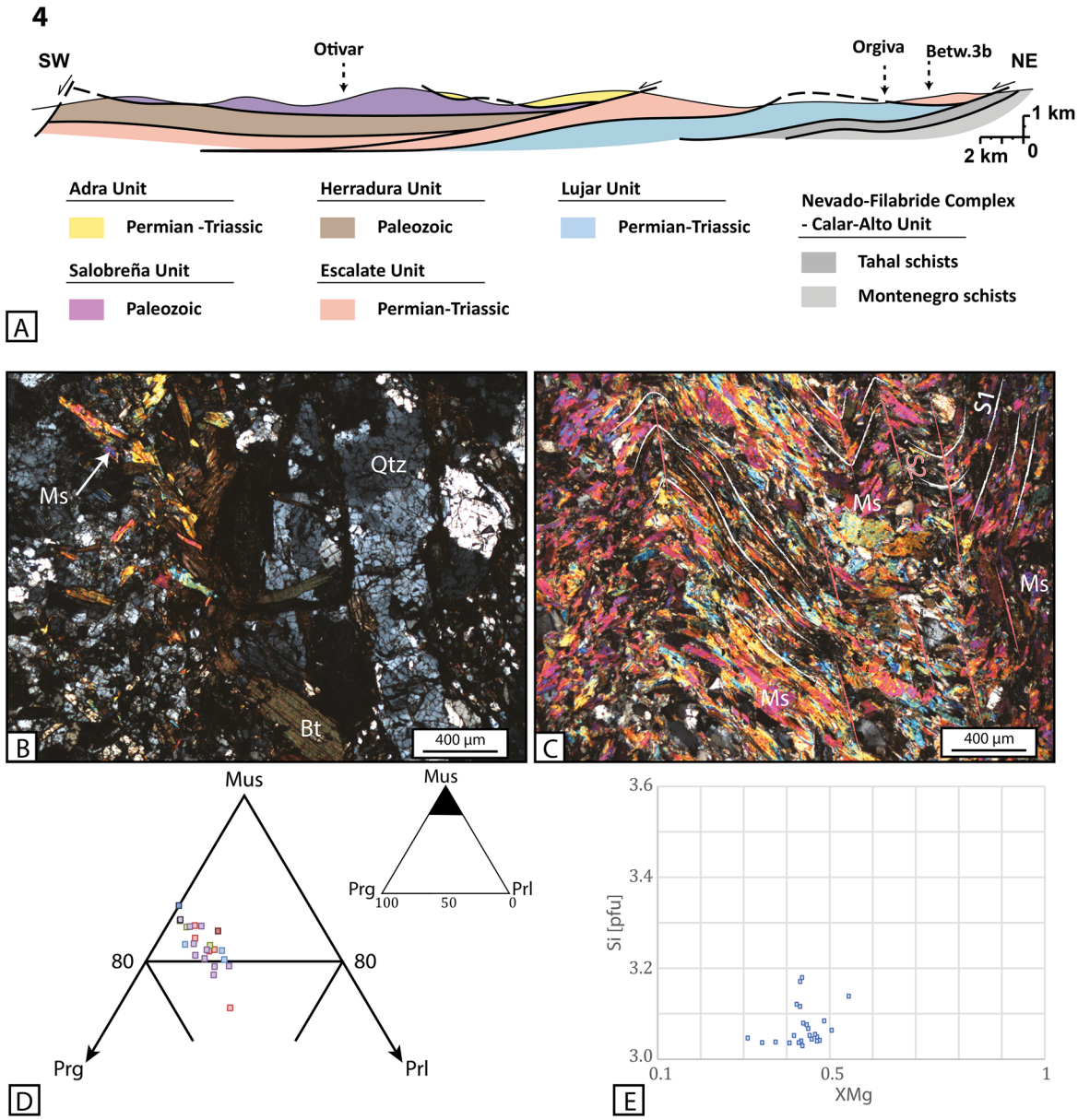

Figure 8. Summary of the structure, petrography and chemical composition for the sample Betw3b. (a) Geological and tectonic cross-section of the sampled area and location of the sample, modified after Azañón et al. (1998). (b and c) Thin-section observations of the dated sample (polarized light). (d) Ternary composition plot for white micas. (e) Variation of X_{Mg} versus Si^{IV} contents in white micas.

fine-grained schist displaying few identifiable minerals, including white micas that are in average smaller than 15 µm (Figures 9b–9d). While the outcrop shows the heterogeneous development of a low angle S2 foliation that marks the main macroscopic cleavage, the main planar fabric observable in the thin section still corresponds to the S1 foliation weakly overprinted by a zonal crenulation cleavage (Figures 9b–9d). Unfortunately, the small grain-size precluded precise chemical analysis (Figure 9d). The vein ALP1702 (Figure 10) contains white micas + quartz + chlorite + kyanite (Figures 10b and 10d–10f). White micas and quartz grains are in textural equilibrium without substantial deformation (Figures 10d–10f), implying growth at least partly after crenulation or folding. The white mica compositions do not show any substantial variability (Figure 10g). X_{Mg} in mica ranges from 0.55 to 0.78, with a clustering around 0.69–0.7 (Table 2 and Figure 10h). Si contents range from 3.10 to 3.33, with a maximum density between 3.18 and 3.26 (Figure 10h). Meta-conglomerates ALP1712 and ALP1713 (Figure 11) are characterized by chlorite + Mg-carpholite + pyrophyllite + quartz in host rock, and quartz + pyrophyllite in veins (Figures 11b and 11c). The host rock is characterized by quartz-rich and mica-rich layers.

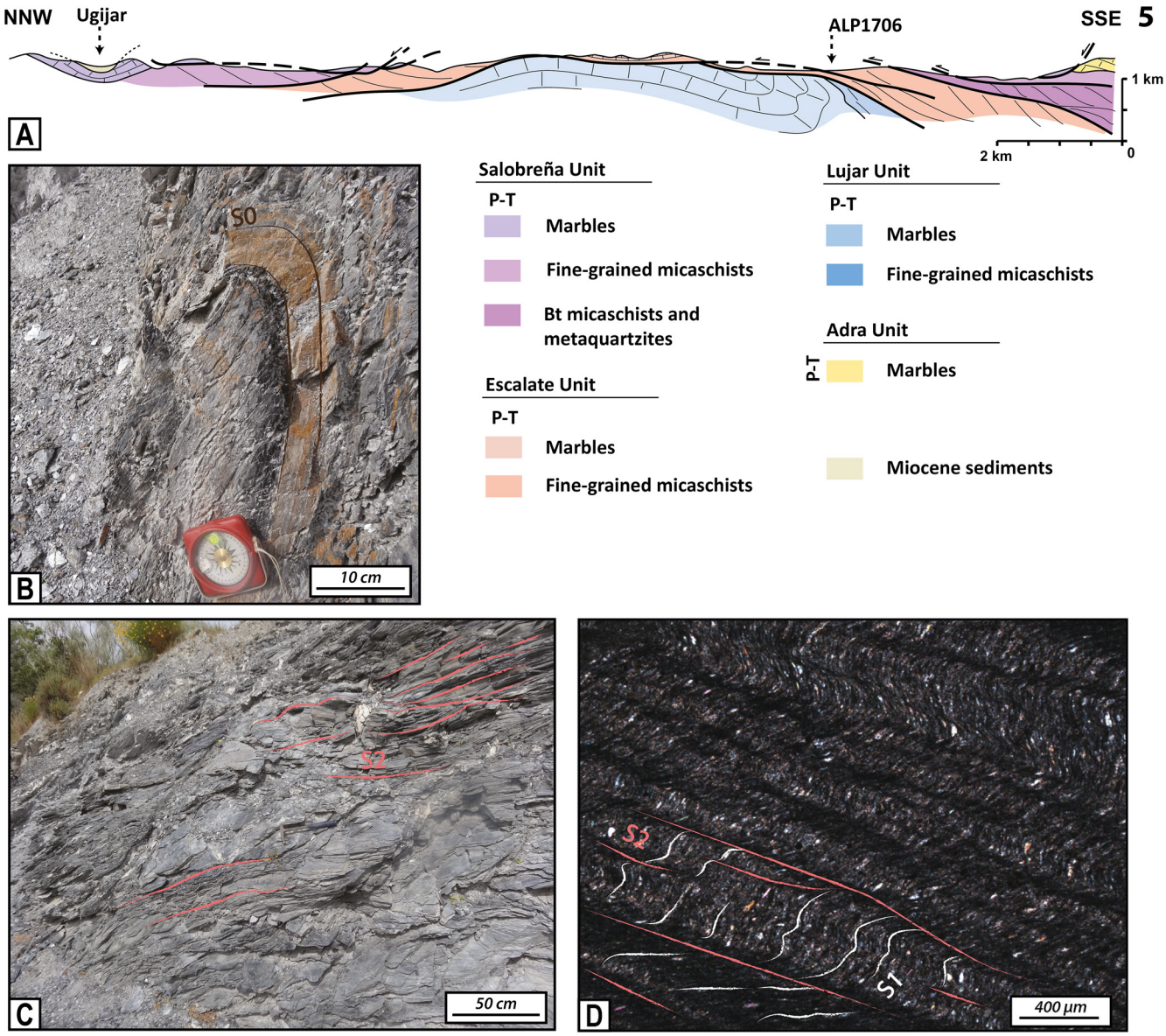

Figure 9. Summary of the structure and petrography observations for the sample ALP1706. (a) Geological and tectonic cross-section of the sampled area and location of the sample, modified after Azañón et al. (1995). (b and c) Outcrop pictures showing the weak development of the S2 and the local preservation of S0. Indicated on the picture c is the location of the sample ALP1706. (d) Thin-section observations of the dated sample (polarized light).

Mica-rich layers present a dominant S1 foliation involved in complex D2 folds with quite large variations in terms of grain-size (Figure 11b). The white micas selected from the vein appear not deformed, similarly to the coarse-grained quartz and pyrophyllite (Figure 11c). Despite the limited number of analyses, white mica composition in veins (i.e., sample ALP1712v) appears homogeneous (Figure 11d), with a Si content between ca. 3.15 and ca. 3.21 and a X_{Mg} varying from ca. 0.28 to ca. 0.35 (Figure 11e). EST1610 sample (Figure 12) also corresponds to a metaconglomerate sample. Mineralogy is mainly limited to quartz, kyanite and white micas (Figures 12b and 12c; Platt et al., 2005) defining the S1 foliation. Quartz and white micas show a quite homogeneous grain-size around 75 µm. White mica composition appears scattered (Figure 12d), X_{Mg} evolving from ca. 0.5 to ca. 0.93 with a homogeneous Si content bracketed between ca. 3.03 and ca. 3.18 (Figure 12e).

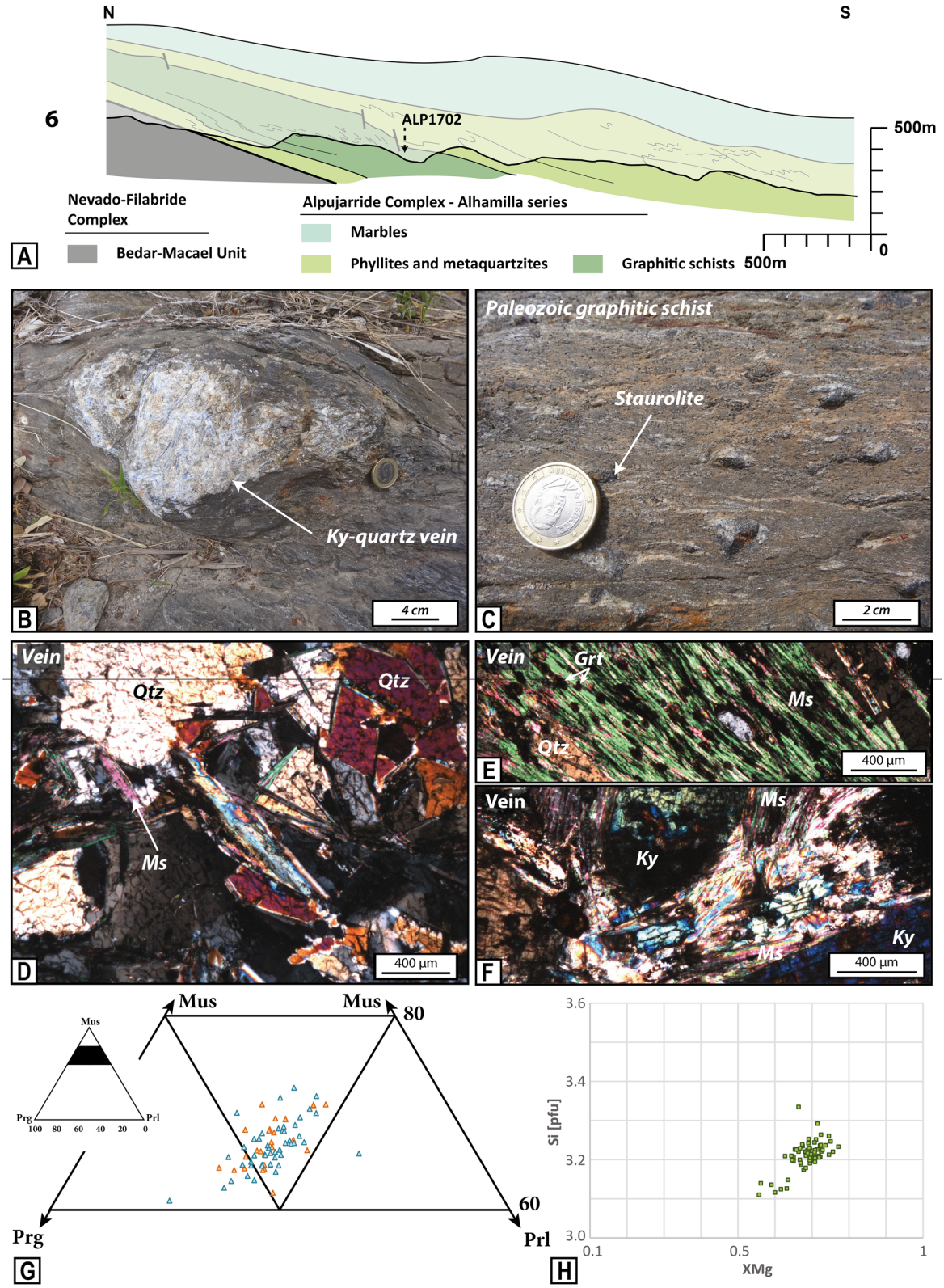

Figure 10. Summary of the structure, petrography and chemical composition for the sample ALP1702. (a) Geological and tectonic cross-section of the sampled area and location of the sample, modified after Platt et al. (1983). (b and c) Outcrop pictures showing a kyanite vein wrapped by the S2 within the host rock. (d–f) Thin section observations of the dated sample (polarized light). (g) Ternary composition plot for white micas. (h) Variation of X_{Mg} versus Si^{IV} contents in white micas.

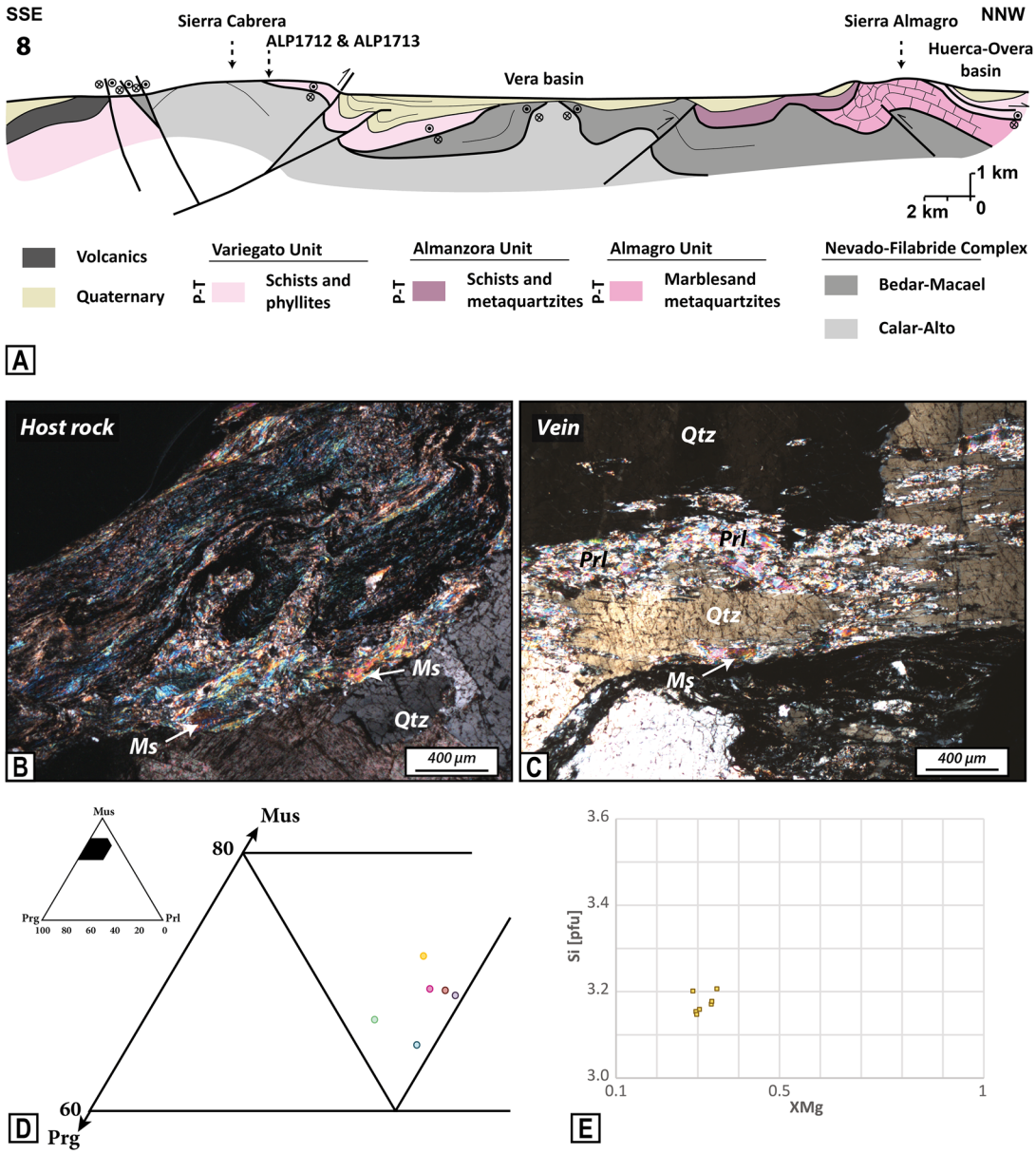

Figure 11. Summary of the structure, petrography and chemical composition for the sample EST1610. (a) Geological and tectonic cross-section of the sampled area and location of the sample, modified after Platt et al. (2005). (b and c) Thin section observations of the dated sample (polarized light). (d) Ternary composition plot for white micas. (e) Variation of X_{Mg} versus Si^{IV} contents in white micas.

5. $^{40}Ar/^{39}Ar$ Age Results

White micas were dated as single grains (size permitting), or mica populations (aggregates) by $^{40}Ar/^{39}Ar$ CO2-laser based step-heating. Aggregates are composed of several coalescing mica flakes extracted directly from the rock by gentle crushing (i.e., as small chips, <100 µg), with their internal textural association preserved. These are single-phase, small-sized populations containing a range of mica crystals in terms of size and, possibly, specific $^{40}Ar/^{39}Ar$ composition or reservoirs. These were collectively degassed as such in vacuo. These aggregates or clusters differ from standard mineral concentrates in that they represent very minute (<<mm^3), coherent, parcels of sample rather than a collection of individual crystals scattered over several dozens of cm^3 (and possibly originating from texturally distinct sites). Details about the procedures of the sample preparation and dating are exposed in the Supporting Information.

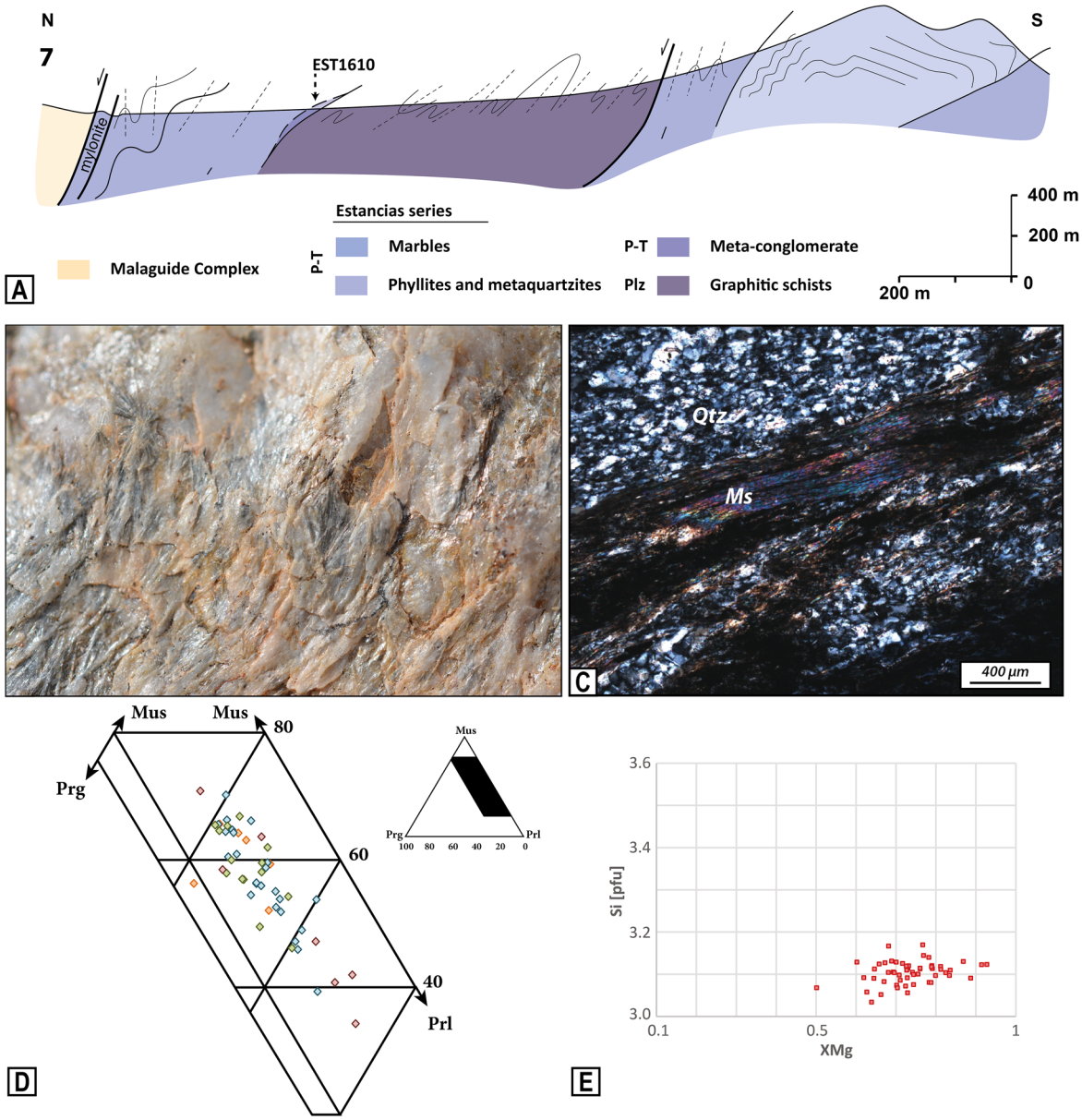

Figure 12. Summary of the structure, petrography and chemical composition for the samples ALP1712 and ALP1713. (a) Geological and tectonic cross-section of the sampled area and location of the samples, modified after Booth-Rea et al. (2005). (b and c) Thin section observations of the dated sample (polarized light). (d) Ternary composition plot for white micas. (e) Variation of X_{Mg} versus Si^{IV} contents in white micas.

Weighted mean ages (WMA) are calculated as integrated (inverse-variance weighted) mean ages over the corresponding steps, and total-gas ages (TGA) by individually summing the Ar isotopes of all steps (equivalent to a K-Ar age). These are quoted at ±1σ. The samples were irradiated for 5 hr in the CLICIT position of the OSU irradiation facility at Corvallis, with the irradiation monitor Fish Canyon sanidine: 28.02 ± 0.28 Ma (Renne et al., 1998), and calculated using interference correction ratios published for this facility (reported in the Supporting Information) along with the isotope decay constants in Steiger and Jäger (1977).

$^{40}Ar/^{39}Ar$ age results are shown in Table 1, summarized in Figures 13 and 14, and presented according to location in Figure 1. Total Gas Ages from the central and eastern part of the chain are scattered between 18.1 ± 0.2 Ma (sample ALP1712v) and 38.2 ± 0.4 Ma (sample TREV.1).

Aggregate TREV.1 was dated twice and provided two concordant total-gas ages of 37.9 ± 0.4 Ma and 38.2 ± 0.4 Ma with rather similar weighted mean age and flat patterns in both spectra. In addition, total fusions

Table 2
Chemical Composition of Several White Micas From the Most Representative Samples (wt %)

	TREV.1				ALP1601h				ALP1601v			ALP1702			
	Mus	Mus	Mus	Mus	Mica	Mica	Mica	Mica	Mus	Mus	Mus	Mus	Mus	Mus	Mus
SiO_2	46.99	47.28	47.81	48.03	45.30	46.55	44.96	46.41	48.02	47.91	47.44	48.12	47.71	48.58	47.99
TiO_2	0.05	0.12	0.05	0.08	0.14	0.11	0.04	0.12	0.10	0.15	0.02	0.46	0.52	0.56	0.63
Al_2O_3	35.48	35.02	35.02	35.31	39.09	39.87	37.88	39.05	35.17	35.11	35.54	32.99	33.14	33.22	33.46
FeO	2.35	2.19	2.35	2.07	1.20	1.14	1.37	0.99	1.94	2.07	1.83	1.28	1.04	1.32	1.22
MnO	0.01	0.05	−0.01	−0.01	−0.04	−0.01	0.02	0.00	−0.03	−0.03	−0.02	0.01	0.05	0.00	0.00
MgO	0.57	0.62	0.68	0.69	0.30	0.27	0.44	0.25	0.57	0.61	0.58	1.66	1.47	1.79	1.27
CaO	0.00	0.02	0.02	0.00	0.99	0.92	0.44	0.46	0.08	0.05	0.34	0.02	0.03	0.03	0.05
Na_2O	0.87	0.63	0.72	0.74	4.27	4.64	4.45	5.66	1.66	1.48	1.73	1.01	1.13	1.06	0.95
K_2O	9.75	9.35	9.63	9.48	3.37	3.15	2.71	2.12	8.22	8.19	7.74	7.97	7.87	7.98	8.14
Total	96.08	95.29	96.27	96.39	94.60	96.64	92.32	95.06	95.73	95.55	95.20	93.51	92.95	94.54	93.71
Atom site distribution (11ox)															
Si	3.10	3.13	3.14	3.14	2.95	2.97	2.99	2.99	3.15	3.15	3.12	3.21	3.20	3.21	3.20
Al	2.76	2.73	2.71	2.72	3.00	3.00	2.97	2.97	2.72	2.72	2.76	2.59	2.62	2.58	2.63
FeMg	0.19	0.18	0.20	0.18	0.09	0.09	0.12	0.08	0.16	0.17	0.16	0.24	0.20	0.25	0.19
K	0.82	0.79	0.81	0.79	0.28	0.26	0.23	0.17	0.69	0.69	0.65	0.68	0.67	0.67	0.69
Na	0.11	0.08	0.09	0.09	0.54	0.57	0.57	0.71	0.21	0.19	0.22	0.13	0.15	0.14	0.12
XMg	0.30	0.33	0.34	0.37	0.32	0.30	0.36	0.31	0.35	0.35	0.36	0.70	0.71	0.71	0.65

Note. Analyses have been realized with a SX Five Cameca microprobe.

were performed on isolated single grains and small mica populations. These define a homogenous (linear) array in a Gauss-plot (Table 1 and Figure 13a, right insert) with a concordant mean age of 36.8 ± 0.4 Ma, consistent with the step-heating ages. Aggregate ALP1601h was dated twice and provided two similarly discordant spectra with consistent total-gas ages of 30.2 ± 0.3 Ma and 29.8 ± 0.3 Ma (Table 1 and Figure 13b). The first experiment shows step ages from c. 18 to c. 51 Ma. The second spectrum shows step ages also evolving from c. 19 Ma to 42 Ma. Both experiments provided two flat-like portions, around 19–20 Ma and 36–40 Ma (Figure 13b). Mica population ALP1601v yielded a total-gas age of 20.3 ± 0.2 Ma (Table 1 and Figure 13b). Aggregate ALP1602h was dated twice, yielding two consistently discordant spectra with a total-gas age of 21.2 ± 0.2 Ma and 21.9 ± 0.2 Ma (Table 1 and Figure 13b). The apparent age increases throughout from 18 to 23 Ma in both cases. Aggregate ALP1602v yielded a total-gas age of 19.6 ± 0.2 Ma (Table 1 and Figure 13b). Two single grains from ALP1702v yielded two mutually discordant spectra with a total-gas age of 15.7 ± 0.4 Ma and 19.5 ± 0.2 Ma (Table 1 and Figure 13c). One is concordant with a WMA age at 19.52 ± 0.04 Ma over 100% of the total ^{39}Ar released. The other yielded an internally discordant spectrum with a broadly concave-upward shape with significantly younger final ages.

Aggregate ALP1603 provided a discordant spectrum with a total-gas age of 20.4 ± 0.2 Ma (Table 1 and Figure 14a). Mica Aggregate Betw3b gave a relatively flat age spectrum with a total-gas age of 18.9 ± 0.2 Ma with an associated WMA of 18.9 ± 0.03 Ma, corresponding to 62% of the total ^{39}Ar released (Table 1 and Figure 14a). Aggregate ALP1706 has been dated twice and provided two broadly similar spectra gradually increasing from 14 to 75–85 with two distinct total-gas age of 41.6 ± 0.5 Ma and 52.7 ± 0.6 Ma (Table 1 and Figure 14b). Two mica aggregates from EST1610 show two different age spectra (Table 1 and Figure 14c), one progressively increasing from 20 Ma to more than 40 Ma (total-gas age = 24.1 ± 0.3 Ma), the second much flatter with a total-gas age of 22.5 ± 0.3 Ma. Two mica aggregates from ALP1713h also provided two discordant spectra with a total-gas age of 22.3 ± 0.3 Ma and 20.4 ± 0.3 Ma (Table 1 and Figure 14d). As for the other discordant spectra of this series, these spectra share a common initial age (around 15 Ma here) and progressively deviate from the initial value as gas extraction proceeds (up to around 25–30 Ma). Aggregate ALP1712v shows a much more regular pattern with

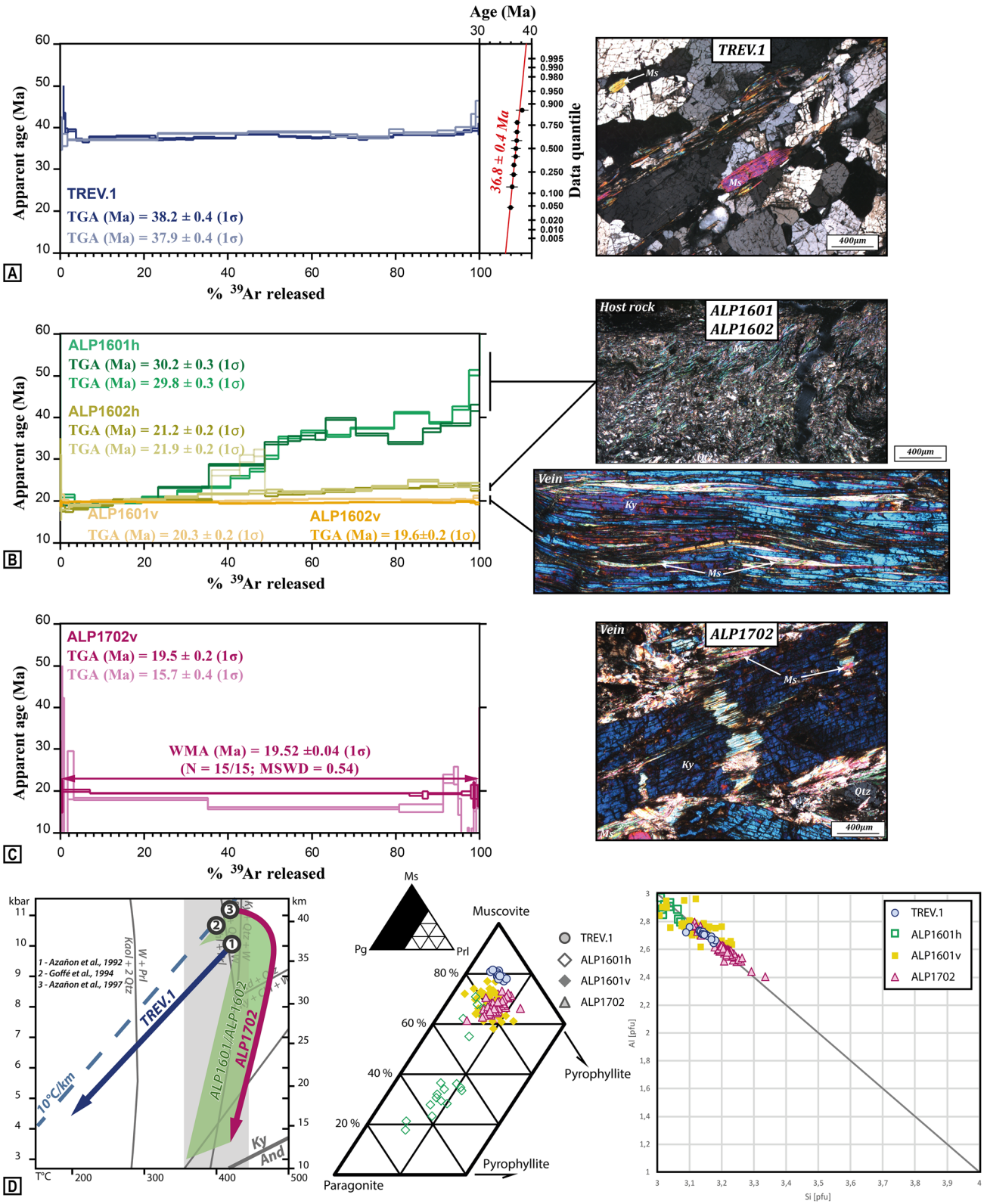

Figure 13. Overview of the $^{40}Ar/^{39}Ar$ age spectra of the most representative samples and the associated petrological, geochemical observations. (a) $^{40}Ar/^{39}Ar$ age spectra obtained and petrological observations for TREV.1 sample. (b) $^{40}Ar/^{39}Ar$ age spectra obtained and petrological observations for ALP1601 and ALP1602 samples. (c) $^{40}Ar/^{39}Ar$ age spectra obtained and petrological observations for ALP1702 sample. (d) *P-T* paths and geochemical data of the detailed samples in (a–c).

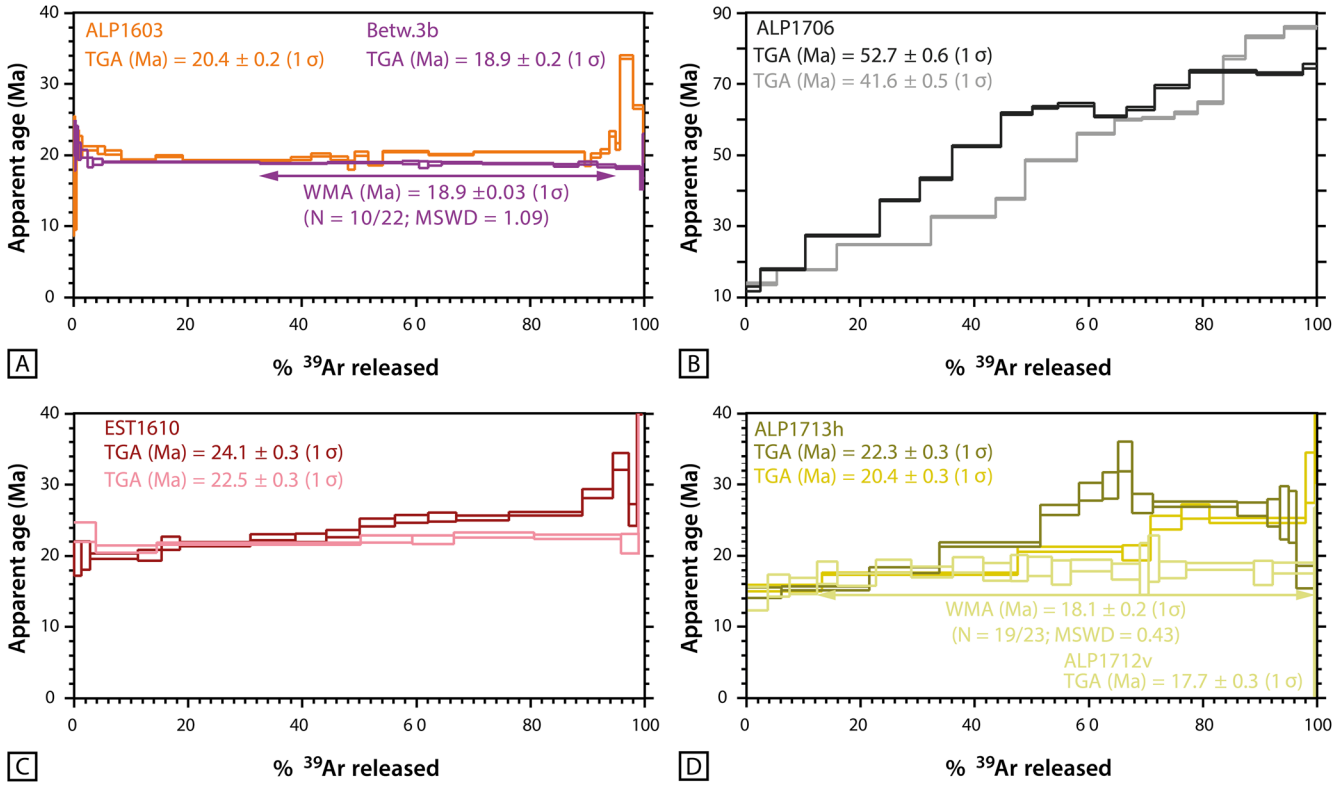

Figure 14. $^{40}Ar/^{39}Ar$ age results for the other samples. Results include spectra from ALP1603, Betw3b, ALP1706, EST1610, ALP1713 and ALP1712 samples.

a flat segment at 18.1 ± 0.2 Ma, corresponding to 88% of the total ^{39}Ar released, with a concordant total-gas age of 17.7 ± 0.3 Ma (Table 1 and Figure 14d).

6. Discussion

Considering the data as a whole, our $^{40}Ar/^{39}Ar$ experiments, combined to those from Monié et al. (1994), reveal two markedly contrasted situations. While age spectra from the westernmost samples show reasonably flat patterns collectively converging to 20 Ma, the easternmost samples from the central and eastern Alpujárride Complex are generally discordant with variably older apparent ages progressively increasing throughout gas release till values up to 50 Ma (i.e., ALP1601h) or higher (80 Ma, ALP1706; Figures 13 and 14).

Most notable is the preservation of homogeneous near-plateau ages around 38 Ma for the sample with the best-preserved H*P*-L*T* parageneses related to the M1 metamorphic conditions (Figure 13a), a component that is also partly preserved in other samples featuring less well-preserved H*P*-L*T* assemblages. Such contrasting patterns may either reflect regional variations in cooling/closure history imposed by the thermal-structural evolution of the host tectonic unit, or crystal-structure plus Ar inheritance effects controlled by the mineralogy, the host lithology and the sample *P-T-t* path.

Both spectra types (plateau-dominated in the western part, and variably discordant in the central and eastern samples) also differ in their specific regional context. Samples showing WMA around 20 Ma in the western Alpujárride Complex display parageneses diagnostic of the late H*T*/L*P* M2 metamorphic overprint, including post-kinematic andalusite growth in the Paleozoic rocks. Those showing variably discordant spectra are associated with early M1 relics that partially escaped M2 overprinting during post-orogenic exhumation (Figure 15; Azañón, 1994; Azañón & Crespo-Blanc, 2000; Booth-Rea et al., 2005; Goffé et al., 1989; Simancas, 2018). The best-preserved H*P*/L*T* paragenesis found in sample TREV.1 provides two concordant Eocene total-gas ages with near-plateau release patterns in addition to fairly concordant total fusion ages (Figure 13). Such an Eocene age has been suspected for a long time—but never fully documented—for the M1 H*P*/L*T* metamorphic event (Monié

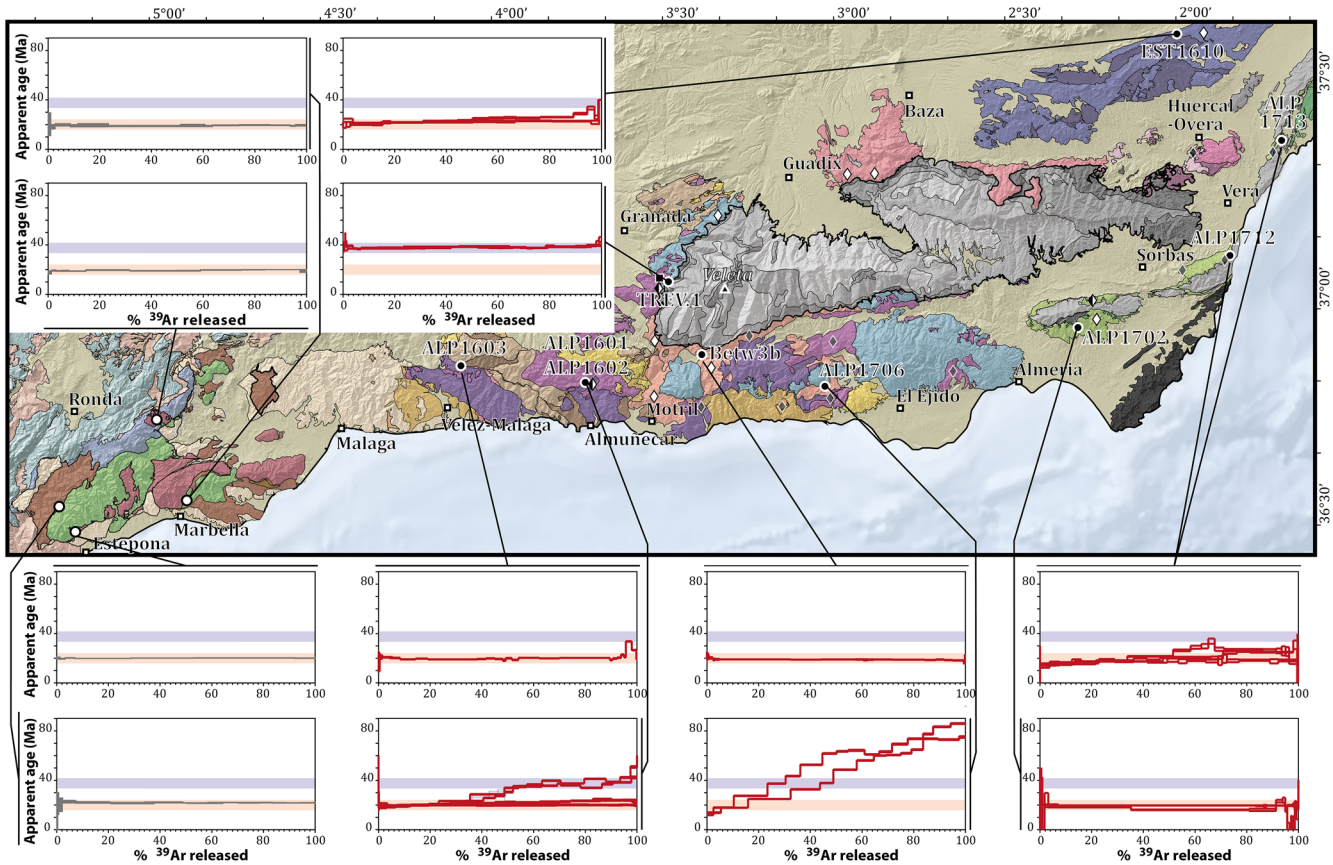

Figure 15. Map of the entire Internal Zones of the Betic Cordillera associated with the $^{40}Ar/^{39}Ar$ age spectrum and according their location. The red-colored spectra are from this study and the black-colored spectra, located mostly in the western part of the complex, are from Monié et al. (1994).

et al., 1991; Platt et al., 2005). Here and for the first time, it is recorded by concordant $^{40}Ar/^{39}Ar$ systematics directly associated to a diagnostic H*P*/L*T* mineralogy. This component appears to have been erased in the less well-preserved H*P*-L*T* parageneses due to the regional H*T*/L*P* overprint. The origin of these general $^{40}Ar/^{39}Ar$ relationships are discussed in the next section in connection with the petrography and structural significance of the samples across the mapped regional trends.

6.1. Significance of $^{40}Ar/^{39}Ar$ and Deformation-Metamorphic Relationships

As stated in Section 5, three main deformation stages (D1, D2, D3) are recognized in the Alpujárride Complex in connection with its *P-T* evolution. H*P*/L*T* metamorphic relics, developed during M1 metamorphic conditions, are associated with a D1 fabric at conditions symptomatic of syn-orogenic exhumation within a *P/T* gradient typical of subduction without wholesale thermal reheating. A D2 fabric is associated with post-orogenic (extensional) nearly isothermal decompression, characteristic of M2 metamorphic conditions, including a local and limited reheating under greenschist- to amphibolite-facies conditions, as testified by the widespread crystallization of sillimanite + staurolite and then andalusite during exhumation (Figure 2; Azañón & Crespo-Blanc, 2000; Azañón et al., 1997; Booth-Rea et al., 2005). A D3 folding phase occurred, corresponding to a crustal contraction due to nappe stacking, responsible for the crenulation and regional folding of D2 fabrics (Azañón & Crespo-Blanc, 2000).

Among the syn- to post-M2 white micas sampled for dating, ALP1603 (Herradura unit) provides a relatively flat age spectrum of c. 20 Ma (Figures 14a and 15), broadly consistent with the muscovite $^{40}Ar/^{39}Ar$ WMA of 18.3 ± 0.3 Ma obtained by Monié et al. (1994) in the same area from the same tectonic unit. Syn- to post-D2 white micas taken from veins ALP1601v and ALP1602v (Salobreña unit) also give more internally discordant spectra fluctuating around 20 Ma (Figures 13b and 15). The best-behaved white mica Betw.3b (Escalate unit)

gives a statistically acceptable and similar WMA at 18.90 ± 0.03 Ma (Figures 14a and 15) that is consistent with the phengite WMA of 19.5 ± 0.5 Ma obtained by Monié et al. (1991) in the same area. Overall, similar young ages between 19.52 ± 0.04 Ma (ALP1702v vein, Sierra Alhamilla; Figures 13c and 15) and 18.1 ± 0.2 Ma (ALP1712v, Sierra Cabrera; Figures 14d and 15) are characteristic of those reasonably flat spectra we have obtained for the eastern Alpujárride Complex units. Noteworthy, the most discordant spectra of the entire sample suite always share with the other samples a similar initial age around 18–20 Ma (occasionally younger, 15 Ma, for ALP1713h and ALP 1706).

In terms of internal isotopic disturbance, we note a systematic trend of steadily increasing apparent ages as the degree of discordance and extent of degassing increase in these samples. The resulting staircase pattern is reminiscent of partial ^{40}Ar loss/retention or slow cooling (Beaudoin et al., 2020; Harrison & Lovera, 2014). Slow cooling in the Ar-muscovite closure interval over more than 20 Myr (e.g., ALP1601h; Figure 13b) can be safely discarded given the documented *P-T* paths and the tectonic context. We interpret this pattern as reflecting partial retention/resetting of a primary radiogenic component (first closure age or inherited pre-metamorphic component) that was variably to almost completely reset through the D2 stage because of the M2 H*T*/L*P* metamorphic conditions. The extent of resetting was variable according to the starting protolith, mineralogy and, most importantly, structural setting.

The case for partial Ar resetting does make sense in the context of the H*P* samples that experienced crystallization conditions just within - or in a range slightly above - the nominal closure interval for Ar retention in white mica near 400°C (Harrison et al., 2009). At M1 H*P*/L*T* metamorphic conditions, pressure effects can come into play to reduce diffusivity and enhance retentivity, as shown by static residence-time modeling by Warren et al. (2012). Such theoretical calculations predict more than 95% retention of initial (pre- or syn-H*P*) radiogenic ^{40}Ar at peak-temperature conditions of 420 ± 30°C and peak-pressure conditions of 9 ± 2 kbar and grain-sizes pertinent to TREV.1 white micas (1.0–0.5 mm), even for static holding times in excess of 10 Myr. In contrast, the highest grade sample (ALP1603: 11 ± 1 kbar, 580 ± 40°C) would have endured more extensive equilibration equivalent to a loss greater than 95% for the same grain-size and holding time at H*P*. No matter how crude, these estimates serve to illustrate that M1 H*P*/L*T* metamorphic conditions in the Alpujárride Complex were critically close to closed-system behavior of Ar in white mica already at peak metamorphic conditions. Above all, they argue in support of potential retention of early (syn-H*P*) ^{40}Ar/^{39}Ar closure ages, as presumably recorded by TREV.1 white micas.

The case for enhanced retentivity due to moderate peak-*T* Alpine conditions is also supported by the data from ALP1706 white micas. This sample displays two reproducible staircase age spectra (Figure 14b) with initial low-T ages around 15 Ma in line with most of the samples. However, the two spectra differ by reaching much older final ages in excess of 80 Ma. This is well above what is commonly recorded by ^{40}Ar/^{39}Ar dating elsewhere in the Betics. Primary (pre-resetting) closure ages of such an antiquity are difficult to fit into the realm of the Alpine H*P*/L*T* evolution. This calls for an alternative explanation invoking either pre-metamorphic ^{40}Ar inheritance (e.g., de Jong, 2003) or excess ^{40}Ar (e.g., de Jong et al., 2001). While we have no independent evidence to prefer one over the other, the first option is consistent with the host unit being made of very low-grade phyllites from the Rio Grande (Sierra de Gador, see Figure 9). These stayed below <420°C, and show only very fine-grained small white micas (Figures 2 and 9). We thus interpret these spectra as recording partial resetting of a pre-metamorphic (i.e., detrital) component in the same way as Platt et al. (2005) concluded that partial resetting of detrital grains prevailed in samples from the same low-grade phyllites. Note that these authors interpreted in situ ^{40}Ar/^{39}Ar ages in a similar low-grade phyllite from the Sierra Alhamilla as the age of the H*P*/L*T* event around 48 Ma. These low-grade phyllites experienced peak-temperature conditions around 300°C (Martínez-Martínez & Azañón, 1997; Platt et al., 2005), too low to permit substantial growth of new white micas from former mica precursors (Akker et al., 2021; Hueck et al., 2020; Sanchez et al., 2011). Also, fission-tracks ages from zircon with admittedly lower opening/closure temperature than the ^{40}Ar/^{39}Ar system (Fission-tracks *Tc* zircon is comprised between 260 and 360°C; Bernet, 2009; Guedes et al., 2013; Tagami & Shimada, 1996) appear largely unreset in the same area. Together with the heterogeneous spatial distribution of in situ ages (Platt et al., 2005), this indicates that these phyllites behaved like those with old ages from the Rio Grande area, and that they recorded a partial resetting of an older (detrital) component (that is indeed described in their sample).

Along with TREV.1 results, these observations thus argue in support of partial to complete retention of pre- and peak-metamorphic ^{40}Ar/^{39}Ar ages due to subdued diffusion at the relatively low temperatures reached during

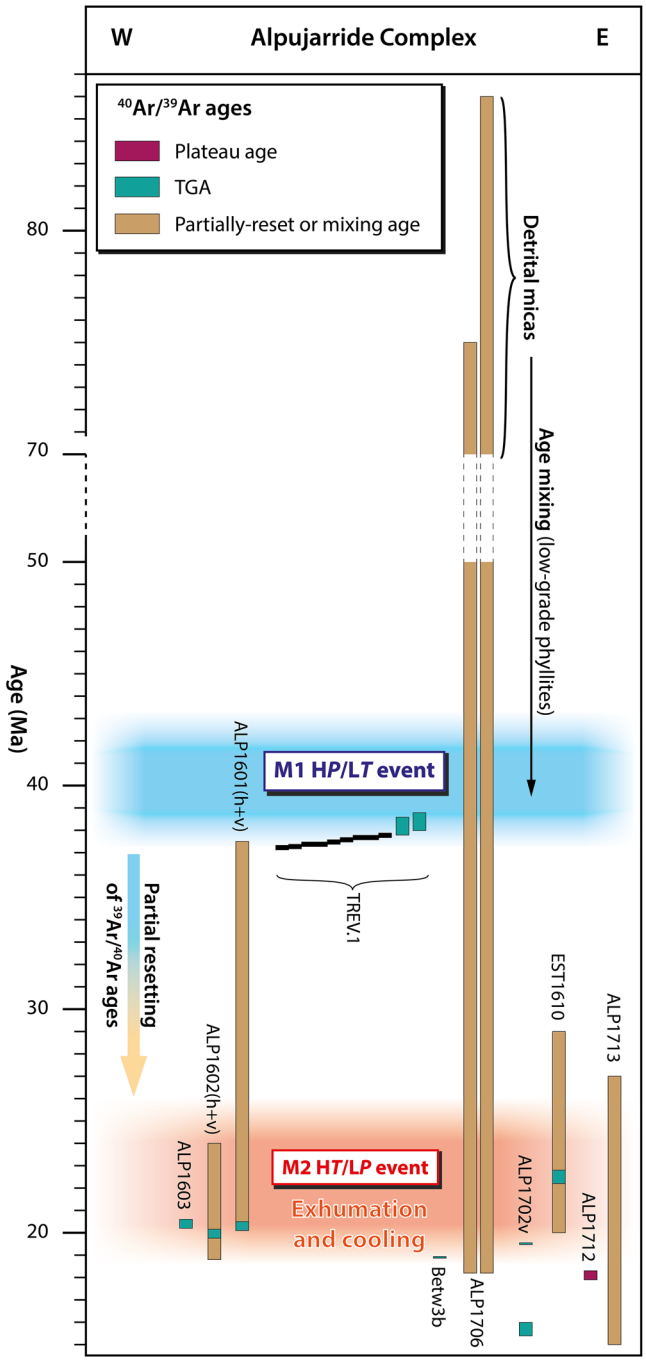

Figure 16. Time-chart compiling the $^{40}Ar/^{39}Ar$ ages results obtained in this study. Proposed are the climax periods for both the M1 high-pressure/low-temperature (H*P*/L*T*) and the M2 H*T*/L*P* metamorphic events recorded by the whole Alpujárride Complex.

the early (peak-pressure) Alpine event and we attribute the staircase spectrum pattern obtained on the other disturbed samples to a subsequent resetting of this primary component. Most probably, such resetting was not purely thermal-diffusion driven, however. In keeping with recent UV-laser probe $^{40}Ar/^{39}Ar$ studies documenting subgrain-scale ^{40}Ar disequilibrium patterns developed in dynamically exhumed and overprinted peak-pressure phengites (Beaudoin et al., 2020; Laurent et al., 2021), our data show that resetting occurred in a way locally combining deformation along with thermal-decompression effects regionally defining a major event at 20 Ma.

ALP1601h is particularly relevant in this regard. This sample texturally records only one white mica generation post-dating M1, but pre-dating M2 (Figures 6d and 13b) and provides two very similar duplicate spectra (Figure 13b). In contrast, the companion white mica ALP1601v sampled from a secondary (undeformed) vein nearby in the same outcrop (Figures 6e and 13b) records much younger and more homogeneous apparent ages at 20.3 ± 0.2 Ma (Figure 13b). These age-geometry relationships are fully consistent with the structural setting of these two texturally distinct samples. They suggest that the syn- to late-D2 emplacement of the vein near 20 Ma was associated with partial resetting of the M1 white micas in the host micaschists, and that the latter crystallized and went through closure between M1 and M2, presumably round 38 Ma (Figures 13, 16 and 17).

The consistent old/young relationships between the host/vein pairs of samples ALP1713h/ALP1712v (Figure 14d) and ALP1602h/ALP1602v (Figure 13b) illustrate the same trend and mechanism. The staircase spectra of ALP1602h, ALP1713h, and EST1610 can be interpreted similarly as partial and variable resetting. This is more pronounced for ALP1602h than for ALP1601h with a primary (i.e., relic) age depressed to a residual component as young as 24 Ma, similar to ALP1713h and EST1610 (compare Figure 13b and Figures 14c and 14d). This common feature demonstrates that the extent of resetting was variable at the sample scale since the duplicates are within ~ mm of each other in each sample. This implies the combination, at least locally, of several mechanisms involving volume diffusion, deformation, grain-size, and fluid transfer to explain the variable extent of resetting as extensively discussed elsewhere and further below (Beaudoin et al., 2020; Laurent et al., 2021, and references therein). Platt et al. (2005) previously noted similar age relationships in the phyllites from the Sierra de las Estancias, with old ages around 45 Ma and younger ages around 19 Ma that they related to the proximity to an extensional detachment possibly responsible for the rejuvenation of the isotopic system.

6.2. Retention Kinetics During Overprinting: *P-T* and Structural Effects

As discussed in Section 6.1, we do not rely on nominal or tailored closure temperatures to explain the $^{40}Ar/^{39}Ar$ ages in a Dodsonian sense (Dodson, 1973). We rather refer to the concept of critical ^{40}Ar retention *P-T* fields calibrated in terms of grain-size and static residence time (Warren et al., 2012). Integrating the residence time in the net Ar loss/retention balance is much more informative and relevant than prescribing a cooling rate to compute a theoretical closure-*T*. The Dodsonian formalism strictly assumes cooling linear in t^{-1} from infinitely high - hence unrealistic - temperatures to force zero initial ^{40}Ar and cooling-only retention kinetics. In contrast, static-isothermal retention kinetics predicted at peak *P-T*

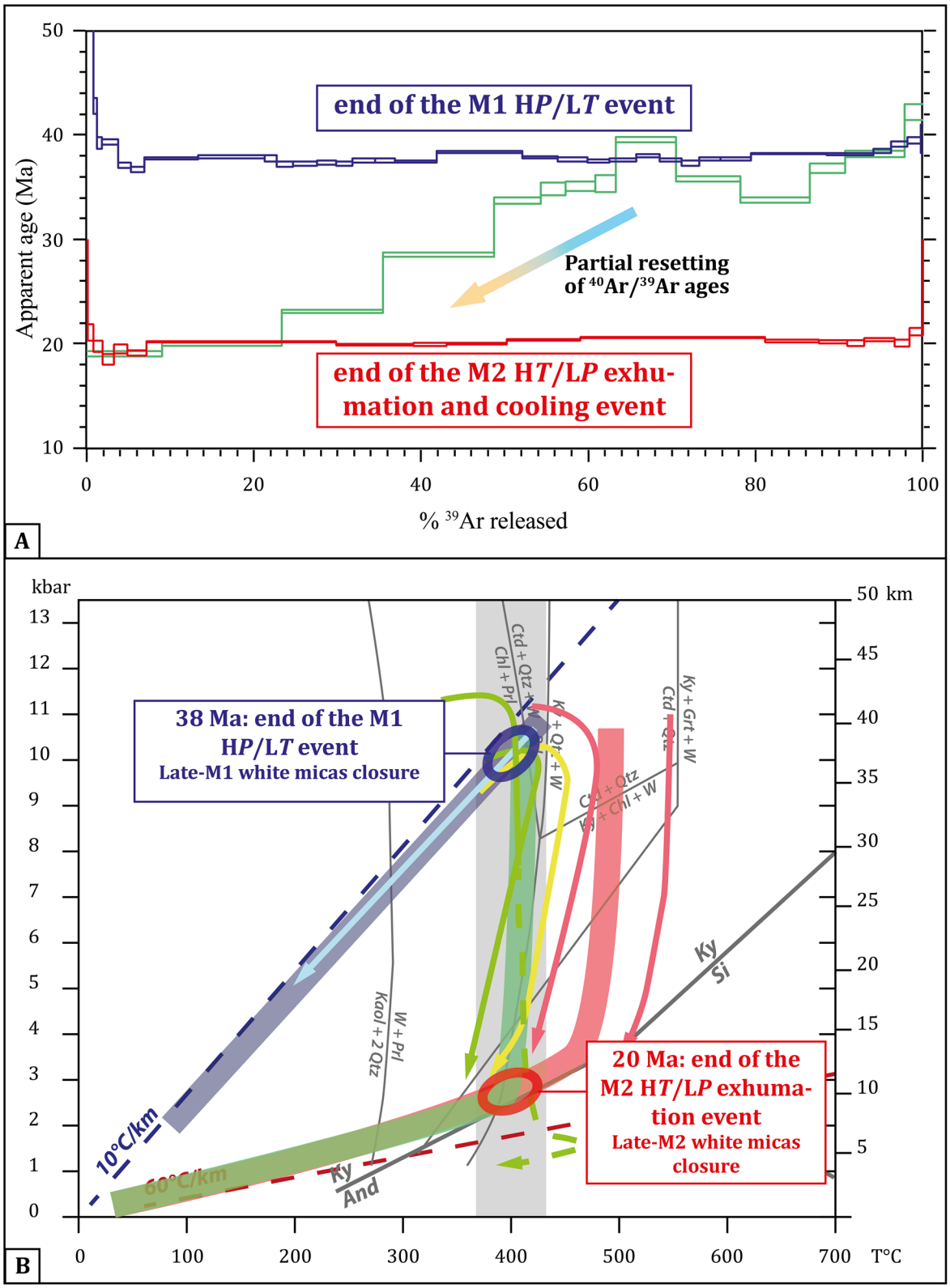

Figure 17. End-members $^{40}Ar/^{39}Ar$ age spectra and their relationships with the main metamorphic events affecting the Alpujárride Complex.

conditions provides a maximum bound to be placed on the permissible age retained at those conditions based on the range in mica grain-size (250–500 μm, on average, for most samples) and the *P-T* condition of interest (Figure 3).

In such a context whether the dated micas crystallized below or above a nominal or Dodsonian-type closure-*T* is not pertinent. In particular, we refrain from ascribing a definite *T*-meaning (and a "closure" vs. "crystallization" status) to the corresponding ages because the retention process governed by residence time is fuzzy and potentially affected by other processes controlled by widely varying kinetics and thresholds during dynamic (re)crystallization across the M1-M2 transition (e.g., changing pressure, stress, and transient fluid-rock interactions). A more useful concept to use here is that of dynamic closure whereby different mica generations potentially record the timing of growth/replacement by dissolution-precipitation and stress-induced recrystallization superimposed on first-order thermal effects (Beaudoin et al., 2020). Protracted or episodic mineral (re)crystallization during progressive exhumation and overprinting of H*P*/L*T* metamorphic rocks may result in a mozaic of texturally and isotopically complex crystals often bearing no apparent relationship to mineral chemical composition, microstructure, or overprinting textures (Laurent et al., 2021). Such systematics may be revealed through coupled in situ and step-heating dating only (e.g., Kellett et al., 2017; Scaillet, 1996; Scaillet et al., 1992; Wiederkehr et al., 2009), and requires exhaustive in situ coverage to permit identification of mixed age reservoirs and their potential end-members (Beaudoin et al., 2020; Laurent et al., 2021; Simon-Labric et al., 2009; and references therein).

Although the fine to medium-grained size of our samples precluded such a systematic approach here, these are texturally and geochemically well characterized in terms of their *P-T* and structural evolutions to permit an evaluation of the $^{40}Ar/^{39}Ar$ record in connection with the D1-D2-D3 deformation sequence identified through the belt-building process. In our case, syn to post-M1 to –M2 white micas are sometimes clearly texturally decoupled (e.g., post-kinematic veins), each recording different *P-T-t* snapshots according to location, lithology, and host unit. In particular, we infer variable extent from none-to-complete ^{40}Ar resetting to have occurred due to locally overlapping M1-M2 relationships in combination with exhumation effects in the critical range for Ar retention in white mica. The exhumation path of the different units occurred close to the kinetic transition from fully closed to partially open-system behavior, with TREV.1 traveling back to the surface along a decompression *P-T* path mostly parallel to (but on the low-*T* side, <400°C, Figure 17) of the 95% Ar retention isopleth inferred for such conditions (Warren et al., 2012, their Figures 3 and 4). In contrast, the other pre- to syn-M2 samples underwent variable (re)opening or synkinematic rejuvenation by traveling on the high-*T* side (probably no more than ∼100°C warmer)—or cutting across—such ^{40}Ar retention isopleth, with local effects (grain-size, static-dynamic overprinting, syn-M1 inheritance) producing the full array of $^{40}Ar/^{39}Ar$ ages we observe today.

The lack of systematic correspondence of $^{40}Ar/^{39}Ar$ with texture is a clear manifestation of such effects. The composite fabric seen in ALP1601h (Figure 6) correlates with clear-cut differences in bulk $^{40}Ar/^{39}Ar$ record relative to ALP1601v (Figure 13b; see also ALP1713h, Figures 11b and 14d). This is also reflected by the inheritance effect also correlating with the crenulation fabric of sample ALP1706 (Figures 9 and 14b). The same cannot be said, however, of the texturally composite sample Betw3b (Figure 8c) which is also one providing the flattest $^{40}Ar/^{39}Ar$ release pattern (Figure 14a). Likewise, EST1610 shows a discordant $^{40}Ar/^{39}Ar$ pattern (Figure 14c) but no composite fabric (Figure 12c). Mica composition is sufficiently contrasted in the case of the post-kinematic veins to distinguish different mica generations (Figure 6f), but the grain-size is otherwise too small to document compositional shifts or internal deformation features indicating texturally distinct $^{40}Ar/^{39}Ar$ subdomains due to, for example, passive rotation/realignment versus intracrystalline kinking + subgrain rotation/recrystallization ± segmentation (Figures 6 and 9). The fabric-forming (matrix) micas could not be mechanically separated from this sample to resolve specific $^{40}Ar/^{39}Ar$ reservoirs, suggesting that the locally discordant ages are potentially mixed ages combining partial resetting with neocrystallization. Taken collectively, the $^{40}Ar/^{39}Ar$ results suggest that inheritance and partial resetting effects are locally variable and best accounted for by a mechanism of recrystallization in a context of dynamic closure and re-opening controlled by deformation ± fluids in addition to diffusion, collectively resulting in relicts ± totally reset ages coexisting at the scale of a single specimen.

The finding of Eocene ages in the sample best preserving the H*P*/L*T* parageneses (TREV.1, Figures 13a, 15, 16 and 17) is a major result in this perspective. This primary age is argued to record syn-to-post-M1 dynamic cooling/closure, thereby putting the first robust constraint on the H*P*/L*T* metamorphic event. In contrast, M2 was associated with a major and much later mechanical destabilization of the H*P*/L*T* prism via a switch to back-arc

extension with exhumation through a dominantly nearly isothermal decompression of the Alpujárride Complex unit (Jolivet et al., 2003). As we next discuss, this tectonic switch forced the white mica system well into the ^{40}Ar open-behavior *P-T* field to produce the general ^{40}Ar/^{39}Ar resetting pattern at 20 Ma documented across the whole belt.

6.3. Geodynamic Reconstruction and Implications

The different tectonic units composing the Alpujárride Complex have undergone various peak-pressure conditions along a quite steady subduction *P/T* gradient, as well as different retrograde *P-T* paths during exhumation (Figure 2; Azañón, 1994; Balanyá et al., 1997; Booth-Rea et al., 2005; Goffé et al., 1989; Jolivet et al., 2003; Tubía & Gil Ibarguchi, 1991).

The main crustal thickening phase during subduction is recorded by the first deformation phase D1 (Azañón & Crespo-Blanc, 2000; Balanyá et al., 1997; de Jong, 1991; Goffé et al., 1989; Jolivet et al., 2003; Platt et al., 2005). Despite variable peak *P/T* conditions, almost all Alpujárride Complex units were affected by a nearly isothermal decompression including sometimes limited heating at low pressures (i.e., M2 metamorphic conditions), coeval with the development of the main foliation, S2 (Figures 2 and 6). In some cases, however, for example, the Salobreña and Escalate units near Trevenque Pass, preservation of aragonite testifies for cold temperature conditions during exhumation, hence syn-orogenic exhumation, under H*P*/L*T* conditions (Figures 2 and 4; Azañón, 1994; Azañón et al., 1997), without substantial overprint by later metamorphic events. Our new age-results thus confirm the Eocene ages suspected in earlier studies and clearly link them with the H*P*-L*T* M1 metamorphic event. They reflect the end of the H*P*/L*T* metamorphic event around 38 Ma (Figures 13a, 15, 16 and 17), which can be considered a minimum age for the H*P*/L*T* event. D2 is associated with intense crustal thinning, with crustal unroofing up to 23 km (Azañón, 1994; Azañón et al., 1997). Metamorphic zones indeed appear drastically condensed sub-parallel to S2, which is interpreted as intense shortening perpendicular to the main foliation (i.e., flattening; Azañón, 1994; Balanyá et al., 1997; Platt et al., 2013; Tubía et al., 1997). The development of S2 marks the breakdown of the M1 high-pressure assemblages, associated with the formation of chlorite and a second generation of white micas and pyrophyllite. The second stacking event, D3, occurred soon after late stages of the D2 phase, with the final structuration of the Alpujárride Complex units (Azañón & Crespo-Blanc, 2000). D2 and D3 are associated to slab retreat initiated around 30–35 Ma leading to back-arc extension and exhumation of the Alpujárride Complex unit (Jolivet et al., 2003).

Thus, the exhumation during D2 and under M2 metamorphic conditions occurred through a dominantly nearly isothermal decompression (Jolivet et al., 2003) with recrystallization in the greenschist-facies or amphibolite-facies, or even partial melting, depending on the tectonic units (Acosta-Vigil et al., 2014; Azañón, 1994; Azañón & Crespo-Blanc, 2000; Duggen et al., 2004; Esteban et al., 2011; Jolivet et al., 2003; Monié et al., 1991; Negro et al., 2006; Platt et al., 2005, 2013; Tubía, 1994; Tubía et al., 1997). The clustering of ages at ∼20 Ma suggests that all units were finally exhumed roughly coevaly over a portion of crust as wide as 220 km in map view, and possibly over 300 km considering available dating from the western part of the Alpujárride Complex and their equivalent in the Rif (Morocco; Bessière et al., 2021; Janots et al., 2006; Michard et al., 2006; Monié et al., 1994). The clustering of ages around 20 Ma with well-defined weighted mean ages suggests that post-decompression dynamic cooling/closure must have been fast with minimal second-order effects such as structural inheritance and deformation. According to the recorded *P-T* paths (Figure 17), wholesale syn- to post-exhumation dynamic cooling/closure at 350–400°C occurred across the temperature range of the brittle-ductile transition, indicating coeval fast exhumation into the brittle field at the regional scale. Our ^{40}Ar/^{39}Ar data show that the extent of resetting (up to full rejuvenation then closure) at 20 Ma is locally variable but prevalent across the whole central Alpujárride Complex (Figure 15) indicating this was a major, regional, event associated to the D2 phase. This was recognized earlier by Monié et al. (1994) on samples taken further west (Figure 15). Coeval exhumation of the central and eastern part of the Alpujárride Complex at ∼20 Ma should be put in line with the end of the high-temperature metamorphism in the western part. There, white and black micas were systematically found to provide flat age spectra ranging in the tight interval 21.6–18.7 Ma (weighted mean ages; Figure 15; Monié et al., 1994). Taken collectively, these data argue in favor of a relatively fast and common dynamic cooling/closure through 300–400°C at around 20 Ma across the entire area.

The c. 20 Ma age is also ascribed to thrusting and final emplacement of the Internal Zones, that is, the basement and cover units, on top of the external units (Acosta-Vigil et al., 2014; Do Couto et al., 2016; Duggen et al., 2004;

Jolivet et al., 2003; Mancilla et al., 2015; Negro et al., 2006; Platt et al., 2013; Santamaría-López et al., 2019). This implies that the main cause for this fast regional exhumation is kinematically linked to both back-arc extension and emplacement onto the Iberian margin by thrusting (transported in the hanging-wall of the main structure). Exhumation of the entire region in a short time during the Early Miocene readily explains the collective freezing of the $^{40}Ar/^{39}Ar$ isotopic system at this period for most tectonic units (Bessière et al., 2021). It is a major thermal-kinematic signature that is consistent with fission-tracks ages on zircons and apatites showing that the Alpujárride Complex was almost entirely exhumed to sub-surface conditions around 20 Ma (Figure 3; Esteban et al., 2004; Platt et al., 2005, 2013; Sánchez-Rodríguez & Gebauer, 2000; Tagami & Shimada, 1996). Such a scenario is further consistent with the first sediments unconformably overlying the Alpujárride Complex metamorphic rocks between the Aquitanian and Burdigalian, that is, around 20.5 Ma (Figure 3; Serrano et al., 2007). Only those units exhumed earlier show either WMA-like Eocene ages (e.g., sample TREV.1, Figures 13a, 13d, 15, and 17) or partially reset ages.

As noted Section 6.2, time-residence analysis predicts survival of near peak-*P* $^{40}Ar/^{39}Ar$ retention ages for over ∼10 Myr residence at conditions endured by TREV.1 white micas (Warren et al., 2012), making it difficult to place a precise temporal bound between the effective exhumation of this sample and the subsequent mechanical destabilization of the entire H*P*/L*T* subduction wedge later on. These data imply that the H*P*/L*T* orogenic wedge structure could have survived until at least ca. 28 Ma (=38–10 Myr) to allow full preservation of this age by syn-orogenic exhumation. On the other hand, the relatively cold range of isothermal exhumation paths recorded throughout the eastern-central Alpujárride Complex (Figures 2 and 3) does not allow for any late thermal drive to explain the massive eradication of early (syn-H*P*) ages, suggesting instead a continuum in *P-T* changes. As argued before, both observations are not mutually exclusive and rather imply that resetting was largely driven by a sudden and fast, en-masse, tectonic decompression (±recrystallization) into the ^{40}Ar open-system behavior *P-T* field close to the Aquitanian-Burdigalian boundary producing the general $^{40}Ar/^{39}Ar$ resetting pattern converging at 20 Ma throughout the whole belt.

Thus, in terms of crustal-scale kinematics, the 20 Ma event does not just record a major thermal event but the thermal-kinematic response of a tectonic event far outpacing the rate of conductive cooling by thermal relaxation alone. We relate this major event to back-arc extension in the Internal Zones and transportation in the hanging-wall of the main thrust on top of the External Zones. This is in line with the idea that 20 Ma is approximately the time when the slab started its delamination and tearing with fast westward migration (Jolivet et al., 2006; Mancilla et al., 2015).

7. Conclusion

Our new $^{40}Ar/^{39}Ar$ age data from the Alpujárride Complex lead to the main following conclusions:

1. The well-preserved H*P*/L*T* parageneses, related to the M1 metamorphic event, coeval with the growth of Fe-Mg-carpholite yield weighted mean ages around 38 Ma. These are the first internally consistent ages ever produced for index H*P* mineral associations assigned to the M1 H*P*/L*T* metamorphic event, the early stages of retrogression and syn-orogenic exhumation in these units. The 38 Ma age establishes a younger limit to the M1 metamorphic event when these tectonic units were decoupled from the subducting lithosphere and started their exhumation.
2. A clear regional trend is identified in the magnitude of the syn-extensional reworking and resetting of the white mica $^{40}Ar/^{39}Ar$ systematics, the more easterly samples preserving a blurred signature of their first (post-M1) closure age while a partial to complete eradication of this radiogenic component is progressively established further west in the Ronda massif (Bessière et al., 2021). Along this trend, mixed-type age spectra (plateau-like to staircase-shaped) coexist as the result of sample-scale variations in deformation magnitude and textural overprint; these locally result in variable inheritance of (early to pre-) metamorphic ages. Such a patchy preservation of early (syn-M1) ages due to isotopic mixing/overprinting with syn- to late-M2 resetting ages near 18–20 Ma has for long precluded temporal discrimination of both events.
3. At the scale of the Betic orogen, the resetting pattern merges into a regionally defined “freezing” event culminating around 20 Ma, consistent with previously published ages. The ca. 20 Ma age recorded all over the Betic-Rif orogen corresponds to a major tectonic switch to fast regional exhumation, associated with back-arc

extension and overthrusting of the Internal Zones on the External Zones and the Iberian margin, probably in connection with the inception of slab tearing and westward motion of the arc.

The Eocene age for the M1 H*P*/L*T* metamorphic event had been postulated for a long time (Michard et al., 2006; Monié et al., 1991, 1994; Platt et al., 2005), but never properly dated due to the difficulty of finding well-preserved H*P* relics untouched by the M1 H*T*/L*P* tectono-metamorphic event. Such an Eocene age for the H*P* event awaits further confirmation by dating similar, exceptionally preserved, H*P* relics throughout the Alpujárride complex and their equivalent in the Rif side of the Gibraltar arc. Determination of the age for the H*P* event for the Nevado-Filabride complex remains also a challenge.

Data Availability Statement

All the data set is provided in this paper and available here: https://zenodo.org/record/5522122#.YUtU9uc682w. All the data set is provided and available in this paper.

Acknowledgments
Work undertook at the Institut des Sciences de la Terre d'Orléans (ISTO) and funded by the OROGEN consortium (French Geological Survey [BRGM], CNRS and TOTAL). The Spanish team was financed by project CGL2015-67130- C2-1-R. We thank Ida Di Carlo for the microprobe analysis performed at the ISTO as well as Michel Fialin and Nicolas Rividi for the microprobe analysis performed at CAMPARIS (ISTeP, Sorbonne Université, Paris). Constructive and detailed reviews by Dawn Kellett (GSC, Dartmouth), Dov Avigad (HUJ, Jerusalem) and Yann Rolland (UdS, Le Bourget-du-Lac) as well as efficient handling (and comments) by the Associate Editor Dordje Grujic were extremely helpful to clarify and expand some critical points of the submitted version and are gratefully acknowledged. The $^{40}Ar/^{39}Ar$ laboratory at ISTO was funded and is supported by the ERC Advanced grant RHEOLITH (grant agreement N°290864), the LABEX VOLTAIRE (ANR-10-LABX-100-01), EQUIPEX PLANEX (ANR-11-EQPX-0036), and the Région Centre ARGON projects.

References

Acosta-Vigil, A., Barich, A., Bartoli, O., Garrido, C. J., Cesare, B., Remusat, L., et al. (2016). The composition of nanogranitoids in migmatites overlying the Ronda peridotites (Betic Cordillera, S Spain): The anatectic history of a polymetamorphic basement. *Contributions to Mineralogy and Petrology*, *171*. https://doi.org/10.1007/s00410-016-1230-3

Acosta-Vigil, A., Rubatto, D., Bartoli, O., Cesare, B., Meli, S., Pedrera, A., et al. (2014). Age of anatexis in the crustal footwall of the Ronda peridotites, S Spain. *Lithos*, *210–211*, 147–167. https://doi.org/10.1016/j.lithos.2014.08.018

Agard, P., Augier, R., & Monié, P. (2011). Shear band formation and strain localization on a regional scale: Evidence from anisotropic rocks below a major detachment (Betic Cordilleras, Spain). *Journal of Structural Geology*, *33*(2), 114–131. https://doi.org/10.1016/j.jsg.2010.11.011

Akker, I. V., Berger, A., Zwingmann, H., Todd, A., Schrank, C. E., Jones, M. W., et al. (2021). Structural and chemical resetting processes in white mica and their effect on K-Ar data during low temperature metamorphism. *Tectonophysics*, *800*, 228708. https://doi.org/10.1016/j.tecto.2020.228708

Alonso-Chaves, F. M., & Orozco, M. (2007). Evolución tectónica de las Sierras de Tejeda y Almijara: Colapso extensional y exhumación de áreas metamórficas en el dominio de Alborán (Cordilleras Béticas). *Revista de la Sociedad Geológica de España*, *20*(3–4), 211–228.

Augier, R., Agard, P., Monie, P., Jolivet, L., Robin, C., & Booth-Rea, G. (2005). Exhumation, doming and slab retreat in the Betic Cordillera (SE Spain): In situ $^{40}Ar/^{39}Ar$ ages and P-T-d-t paths for the Nevado-Filabride complex. *Journal of Metamorphic Geology*, *23*, 357–381. https://doi.org/10.1111/j.1525-1314.2005.00581.x

Augier, R., Booth-Rea, G., Agard, P., Martínez-Martínez, J. M., Jolivet, L., & Azañón, J. M. (2005). Exhumation constraints for the lower Nevado-Filabride complex (Betic Cordillera, SE Spain): A Raman thermometry and Tweequ multiequilibrium thermobarometry approach. *Bulletin de la Societe Geologique de France*, *176*(5), 403–416. https://doi.org/10.2113/176.5.403

Augier, R., Jolivet, L., Do Couto, D., & Negro, F. (2013). From ductile to brittle, late-to post-orogenic evolution of the Betic Cordillera: Structural insights from the northeastern Internal Zones. *Bulletin de la Societe Geologique de France*, *184*(4–5), 405–425. https://doi.org/10.2113/gssgfbull.184.4-5.405

Augier, R., Jolivet, L., & Robin, C. (2005). Late Orogenic doming in the eastern Betic Cordilleras: Final exhumation of the Nevado-Filabride complex and its relation to basin genesis. *Tectonics*, *24*(4). https://doi.org/10.1029/2004tc001687

Azañón, J. M. (1992). Nota preliminar sobra la presencia de sudoita en las metapelitas de la unidad de Trevenque, Alpujárrides centrales. *Geogaceta*, *12*, 68–70.

Azañón, J. M. (1994). *Metamorfismo de alta presion/baja temperatura, baja presion/alta temperatura y tectonica del complejo Alpujarride (Cordilleras Betico-Rifenas)* (PhD Thesis). Univ. Granada.

Azañón, J. M., Blanc, A. C., Dueñas, V. G., & Gómez, M. S. (1995). The Alpujárride Complex structure and its contribution to the ESCI-Béticas 2 deep seismic reflection profile interpretation (Alboran domain, Betic chain). *Revista de la Sociedad Geologica de Espana*, *8*, 491–501.

Azañón, J. M., & Crespo-Blanc, A. (2000). Exhumation during a continental collision inferred from the tectonometamorphic evolution of the Alpujarride Complex in the central Betics (Alboran Domain, SE Spain). *Tectonics*, *19*, 549–565.

Azañón, J. M., Crespo-blanc, A., & García-Dueñas, V. (1997). Continental collision, crustal thinning and nappe forming during the pre-Miocene evolution of the Alpujarride Complex (Alboran Domain, Betics). *Journal of Structural Geology*, *19*, 1055–1071.

Azañón, J. M., Crespo-Blanc, A., García-Dueñas, V., & Orozco, M. (1993). Middle Miocene extensional faulting events and Alpujárride units in the central Betics. *Geogaceta*, *14*, 119–122.

Azañón, J. M., García-Dueñas, V., & Goffé, B. (1992). High pressure mineral assemblages in the Trevenque unit (central Alpujarrides, Andalucía). *Geogaceta*, *11*, 81–84.

Azañón, J. M., García-Dueñas, V., & Goffé, B. (1998). Exhumation of high-pressure metapelites and coeval crustal extension in the Alpujarride complex (Betic Cordillera). *Tectonophysics*, *285*, 231–252.

Azañón, J. M., & Goffé, B. (1997a). Ferro-and magnesiocarpholite assemblages as record of high-P, low-T metamorphism in the Central Alpujarrides, Betic Cordillera (SE Spain). *European Journal of Mineralogy*, *9*, 1035–1051.

Azañón, J. M., & Goffé, B. (1997b). High-pressure, low-temperature metamorphic evolution of the Central Alpujarrides, Betic Cordillera (SE Spain). *European Journal of Mineralogy*, *9*, 1035–1051.

Bakker, H. E., Jong, K. D., Helmers, H., & Biermann, C. (1989). The geodynamic evolution of the internal zone of the Betic Cordilleras (south-east Spain): A model based on structural analysis and geothermobarometry. *Journal of Metamorphic Geology*, *7*, 359–381. https://doi.org/10.1111/j.1525-1314.1989.tb00603.x

Balanyá, J. C., García-Dueñas, V., Azañón, J. M., & Sánchez-Gómez, M. (1997). Alternating contractional and extensional events in the Alpujarride nappes of the Alboran domain (Betics, Gibraltar arc). *Tectonics*, *16*, 226–238.

Barich, A., Acosta-Vigil, A., Garrido, C. J., Cesare, B., Tajčmanová, L., & Bartoli, O. (2014). Microstructures and petrology of melt inclusions in the anatectic sequence of Jubrique (Betic Cordillera, S Spain): Implications for crustal anatexis. *Lithos*, *206–207*, 303–320. https://doi.org/10.1016/j.lithos.2014.08.003

Bartoli, O., Acosta-Vigil, A., Tajčmanová, L., Cesare, B., & Bodnar, R. J. (2016). Using nanogranitoids and phase equilibria modeling to unravel anatexis in the crustal footwall of the Ronda peridotites (Betic Cordillera, S Spain). *Lithos*, *256–257*, 282–299. https://doi.org/10.1016/j.lithos.2016.03.016

Bartoli, O., Tajčmanová, L., Cesare, B., & Acosta-Vigil, A. (2013). Phase equilibria constraints on melting of stromatic migmatites from Ronda (S. Spain): Insights on the formation of peritectic garnet. *Journal of Metamorphic Geology*, *31*, 775–789. https://doi.org/10.1111/jmg.12044

Beaudoin, A., Scaillet, S., Mora, N., Jolivet, L., & Augier, R. (2020). In situ and step-heating $^{40}Ar/^{39}Ar$ dating of white mica in low-temperature shear zones (Tenda Massif, Alpine Corsica, France). *Tectonics*, *39*(12), e2020TC006246. https://doi.org/10.1029/2020tc006246

Bernet, M. (2009). A field-based estimate of the zircon fission-track closure temperature. *Chemical Geology*, *259*(3–4), 181–189. https://doi.org/10.1016/j.chemgeo.2008.10.043

Bessière, E., Jolivet, L., Augier, R., Scaillet, S., Précigout, J., Azañon, J. M., et al. (2021). Lateral variations of pressure-temperature evolution in non-cylindrical orogens and 3-D subduction dynamics: The Betic-Rif Cordillera example. *BSGF-Earth Sciences Bulletin*, *192*(1), 8.

Blichert-Toft, J. (1999). Lu-Hf isotope systematics of garnet pyroxenites from Beni Bousera, Morocco: Implications for Basalt origin. *Science*, *283*, 1303–1306. https://doi.org/10.1126/science.283.5406.1303

Booth-Rea, G., Azañón, J. M., Goffé, B., Vidal, O., & Martínez-Martínez, J. M. (2002). High-pressure, low-temperature metamorphism in Alpujarride units of southeastern Betics (Spain). *Comptes Rendus Geoscience*, *334*, 857–865. https://doi.org/10.1016/s1631-0713(02)01787-x

Booth-Rea, G., Azañón, J. M., Martínez-Martínez, J. M., Vidal, O., & García-Dueñas, V. (2005). Contrasting structural and P-T evolution of tectonic units in the southeastern Betics: Key for understanding the exhumation of the Alboran domain HP/LT crustal rocks (western Mediterranean). *Tectonics*, *24*. https://doi.org/10.1029/2004tc001640

Bouybaouene, M. L., Goffé, B., & Michard, A. (1995). High-pressure, low-temperature metamorphism in the Sebtides Nappes, northern Rif, Morocco. *Geogaceta*, *17*, 117–119.

Chalouan, A., Michard, A., El Kadiri, K., Negro, F., De Lamotte, D. F., Soto, J. I., & Saddiqi, O. (2008). The Rif Belt. In *Continental evolution: The geology of Morocco* (pp. 203–302). Springer. https://doi.org/10.1007/978-3-540-77076-3_5

Crespo-Blanc, A., Comas, M., & Balanyá, J. C. (2016). Clues for a Tortonian reconstruction of the Gibraltar Arc: Structural pattern, deformation diachronism and block rotations. *Tectonophysics*, *683*, 308–324. https://doi.org/10.1016/j.tecto.2016.05.045

Crespo-Blanc, A., Orozco, M., & Garcia-Dueñas, V. (1994). Extension versus compression during the Miocene tectonic evolution of the Betic chain. Late folding of normal fault systems. *Tectonics*, *13*(1), 78–88. https://doi.org/10.1029/93tc02231

de Jong, K. (1991). *Tectono-metamorphic studies and radiometric dating in the Betic Cordilleras (SE Spain)-with implications for the dynamics of extension and compression in the western Mediterranean area*. (PhD Thesis). Vrije Universiteit.

de Jong, K. (1992). A new geodynamic model for tite Betie Cordilleras based on P-T-t paths and structural data from the eastern Bede. *Física de la Tierra*, *4*, 77–107.

de Jong, K. (2003). Very fast exhumation of high-pressure metamorphic rocks with excess 40Ar and inherited 87Sr, Betic Cordilleras, southern Spain. *Lithos*, *70*, 91–110. https://doi.org/10.1016/s0024-4937(03)00094-x

de Jong, K., Féraud, G., Ruffet, G., Amouric, M., & Wijbrans, J. R. (2001). Excess argon incorporation in phengite of the Mulhacén Complex: Submicroscopic illitization and fluid ingress during late Miocene extension in the Betic zone, south-eastern Spain. *Chemical Geology*, *178*, 159–195. https://doi.org/10.1016/s0009-2541(00)00411-3

Dewey, J. F., Helman, M. L., Knott, S. D., Turco, E., & Hutton, D. H. W. (1989). Kinematics of the western Mediterranean. *Geological Society, London, Special Publications*, *45*(1), 265–283. https://doi.org/10.1144/gsl.sp.1989.045.01.15

Do Couto, D., Gorini, C., Jolivet, L., Lebret, N., Augier, R., Gumiaux, C., et al. (2016). Tectonic and stratigraphic evolution of the western Alboran Sea Basin in the last 25 Myrs. *Tectonophysics*, *677*, 280–311. https://doi.org/10.1016/j.tecto.2016.03.020

Dodson, M. H. (1973). Closure temperature in cooling geochronological and petrological systems. *Contributions to Mineralogy and Petrology*, *40*(3), 259–274. https://doi.org/10.1007/bf00373790

Dragovic, B., Angiboust, S., & Tappa, M. J. (2020). Petrochronological close-up on the thermal structure of a paleo-subduction zone (W. Alps). *Earth and Planetary Science Letters*, *547*, 116446. https://doi.org/10.1016/j.epsl.2020.116446

Duggen, S., Hoernle, K., van den Bogaard, P., & Harris, C. (2004). Magmatic evolution of the Alboran region: The role of subduction in forming the western Mediterranean and causing the Messinian Salinity Crisis. *Earth and Planetary Science Letters*, *218*, 91–108. https://doi.org/10.1016/s0012-821x(03)00632-0

Durand-Delga, M. (1980). Le cadre structural de la Méditerranée occidentale. In *International Geological Congress* (pp. 67–85).

Egeler, C. G., & Simon, O. J. (1969). Sur la tectonique de la Zone Bétique (Cordillères Bétiques, Espagne). Étude basée sur la recherche dans le secteur compris entre Almería y Vélez Rubio. In *Verhandelingen der Koninklijke Nederlandse Akademie van Wetenschappen* (Vol. 25).

Esteban, J. J., Cuevas, J., Tubía, J. M., Gil Iarguchi, J. I., & Seward, D. (2005). Metamorfismo, exhumación y termocronología de la Unidad de Yunquera (Alpujárrides occidentales, Cordilleras Béticas). *Revista de la Sociedad Geologica de Espana*, *18*, 61–74.

Esteban, J. J., Cuevas, J., Tubía, J. M., Sergeev, S., & Larionov, A. (2011). A revised Aquitania age for the emplacement of the Ronda peridotites (Betic Cordilleras, southern Spain). *Geological Magazine*, *148*, 183–187. https://doi.org/10.1017/s0016756810000737

Esteban, J. J., Cuevas, J., Vegas, N., & Tubía, J. M. (2008). Deformation and kinematics in a melt-bearing shear zone from the western Betic Cordilleras (southern Spain). *Journal of Structural Geology*, *30*, 380–393. https://doi.org/10.1016/j.jsg.2007.11.010

Esteban, J. J., Sánchez-Rodríguez, L., Seward, D., Cuevas, J., & Tubía, J. M. (2004). The late thermal history of the Ronda area, southern Spain. *Tectonophysics*, *389*, 81–92. https://doi.org/10.1016/j.tecto.2004.07.050

Faccenna, C., Becker, T. W., Auer, L., Billi, A., Boschi, L., Brun, J. P., et al. (2014). Mantle dynamics in the Mediterranean: Mediterranean dynamic. *Review of Geophysics*, *52*, 283–332. https://doi.org/10.1002/2013rg000444

Faccenna, C., Piromallo, C., Crespo-Blanc, A., Jolivet, L., & Rossetti, F. (2004). Lateral slab deformation and the origin of the western Mediterranean arcs. *Tectonics*, *23*. https://doi.org/10.1029/2002tc001488

Frasca, G., Gueydan, F., Poujol, M., Brun, J.-P., Parat, F., Monié, P., et al. (2017). Fast switch from extensional exhumation to thrusting of the Ronda Peridotites (South Spain). *Terra Nova*, *29*, 117–126. https://doi.org/10.1111/ter.12255

García-Casco, A., & Torres-Roldán, R. L. (1996). Disequilibrium induced by fast decompression in St− Bt− Grt− Ky− Sil− and metapelites from the Betic Belt (southern Spain). *Journal of Petrology*, *37*(5), 1207–1239.

Goffé, B., Azañón, J. M., Bouybaouene, J. M., & Julien, M. (1996). Metamorphic cookeite in Alpine metapelites from Rif, northern Morocco, and the Betic Chain, southern Spain. *European Journal of Mineralogy-Ohne Beihefte*, *8*, 335–348.

Goffé, B., Baronnet, A., & Morin, G. (1994). La saliotite, interstratifié régulier 1: 1 cookéite/paragonite. Nouveau phyllosilicate du métamorphisme de haute pression et basse température. *European Journal of Mineralogy*, 897–912.

Goffé, B., Michard, A., Garcia-Dueñas, V., González-Lodeiro, F., Monié, P., Campos, J., et al. (1989). First evidence of high-pressure, low-temperature metamorphism in the Alpujárride nappes, Betic Cordilleras (S.E. Spain). *European Journal of Mineralogy*, *1*, 139–142.

Gómez-Pugnaire, M. T., Rubatto, D., Fernández-Soler, J. M., Jabaloy, A., López Sánchez-Vizcaíno, V., González-Lodeiro, F., et al. (2012). Late Variscan magmatism in the Nevado-Filábride Complex: U-Pb geochronologic evidence for the pre-Mesozoic nature of the deepest Betic complex (SE Spain). *Lithos*, *146–147*, 93–111.

Guedes, S., Moreira, P. A., Devanathan, R., Weber, W. J., & Hadler, J. C. (2013). Improved zircon fission-track annealing model based on reevaluation of annealing data. *Physics and Chemistry of Minerals*, *40*(2), 93–106. https://doi.org/10.1007/s00269-012-0550-8

Harrison, T. M., Célérier, J., Aikman, A. B., Hermann, J., & Heizler, M. T. (2009). Diffusion of ^{40}Ar in muscovite. *Geochimica et Cosmochimica Acta*, *73*(4), 1039–1051. https://doi.org/10.1016/j.gca.2008.09.038

Harrison, T. M., & Lovera, O. M. (2014). The multi-diffusion domain model: Past, present and future. *Geological Society, London, Special Publications*, *378*(1), 91–106. https://doi.org/10.1144/sp378.9

Homonnay, E., Corsini, M., Lardeaux, J.-M., Romagny, A., Münch, P., Bosch, D., et al. (2018). Miocene crustal extension following thrust tectonic in the Lower Sebtides units (internal Rif, Ceuta Peninsula, Spain): Implication for the geodynamic evolution of the Alboran domain. *Tectonophysics*, *722*, 507–535. https://doi.org/10.1016/j.tecto.2017.11.028

Hueck, M., Wemmer, K., Basei, M. A., Philipp, R. P., Oriolo, S., Heidelbach, F., et al. (2020). Dating recurrent shear zone activity and the transition from ductile to brittle deformation: White mica geochronology applied to the Neoproterozoic Dom Feliciano Belt in South Brazil. *Journal of Structural Geology*, *141*, 104199. https://doi.org/10.1016/j.jsg.2020.104199

Jabaloy, A., Galindo-Zaldívar, J., & González-Lodeiro, F. (1993). The Alpujárride-Nevado-Fibábride extensional shear zone, Betic Cordillera, SE Spain. *Journal of Structural Geology*, *15*, 555–569. https://doi.org/10.1016/0191-8141(93)90148-4

Janots, E., Negro, F., Brunet, F., Goffé, B., Engi, M., & Bouybaouène, M. L. (2006). Evolution of the REE mineralogy in HP–LT metapelites of the Sebtide complex, Rif, Morocco: Monazite stability and geochronology. *Lithos*, *87*, 214–234. https://doi.org/10.1016/j.lithos.2005.06.008

Johnson, C., Harbury, N., & Hurford, A. J. (1997). The role of extension in the Miocene denudation of the Nevado-Filábride Complex, Betic Cordillera (SE Spain). *Tectonics*, *16*, 189–204. https://doi.org/10.1029/96tc03289

Jolivet, L., Augier, R., Faccenna, C., Negro, F., Rimmele, G., Agard, P., et al. (2008). Subduction, convergence and the mode of backarc extension in the Mediterranean region. *Bulletin de la Societe Geologique de France*, *179*(6), 525–550. https://doi.org/10.2113/gssgfbull.179.6.525

Jolivet, L., Augier, R., Robin, C., Suc, J.-P., & Rouchy, J. M. (2006). Lithospheric-scale geodynamic context of the Messinian salinity crisis. *Sedimentary Geology*, *188–189*, 9–33. https://doi.org/10.1016/j.sedgeo.2006.02.004

Jolivet, L., & Faccenna, C. (2000). Mediterranean extension and the Africa-Eurasia collision. *Tectonics*, *19*(6), 1095–1106. https://doi.org/10.1029/2000tc900018

Jolivet, L., Faccenna, C., Goffé, B., Burov, E., & Agard, P. (2003). Subduction tectonics and exhumation of high-pressure metamorphic rocks in the Mediterranean orogens. *American Journal of Science*, *303*, 353–409. https://doi.org/10.2475/ajs.303.5.353

Kellett, D. A., van Staal, C., Wilson, R. A., & Rogers, N. (2017). The age of salinic deformation constrained by ^{40}Ar/^{39}Ar dating of multiple cleavage domains: Bathurst Supergroup, New Brunswick Appalachians. *American Journal of Science*, *317*(3), 338–368. https://doi.org/10.2475/03.2017.02

Kohn, M. J., Engi, M., & Lanari, P. (2017). Petrochronology. *Methods and Applications, Mineralogical Society of America Reviews in Mineralogy and Geochemistry*, *83*, 575. https://doi.org/10.2138/rmg.2017.83.0

Kurzawa, T., Bröcker, M., Fotoohi Rad, G., Berndt, J., & Lisker, F. (2017). Cretaceous high-pressure metamorphism and low pressure overprint in the Sistan Suture Zone, eastern Iran: Additional temperature estimates for eclogites, geological significance of U-Pb zircon ages and Rb-Sr constraints on the timing of exhumation. *Journal of Asian Earth Sciences*, *147*, 332–344. https://doi.org/10.1016/j.jseaes.2017.07.051

Laurent, V., Scaillet, S., Jolivet, L., Augier, R., & Roche, V. (2021). ^{40}Ar behaviour and exhumation dynamics in a subduction channel from multi-scale ^{40}Ar/^{39}Ar systematics in phengite. *Geochimica et Cosmochimica Acta*.

Li, B., & Massonne, H.-J. (2018). Two tertiary metamorphic events recognized in high-pressure metapelites of the Nevado-Filábride Complex (Betic Cordillera, S Spain). *Journal of Metamorphic Geology*, *36*, 603–630. https://doi.org/10.1111/jmg.12312

Lonergan, L. (1993). Timinig and kinematics of deformation in the Malaguide Complex, internal zone of the Betic Cordillera, southeast Spain. *Tectonics*, *12*, 460–476. https://doi.org/10.1029/92tc02507

Lonergan, L., & White, N. (1997). Origin of the Betic-Rif mountain belt. *Tectonics*, *16*, 504–522. https://doi.org/10.1029/96tc03937

Loomis, T. P. (1975). Tertiary mantle diapirism, orogeny, and plate tectonics east of the Strait of Gibraltar. *American Journal of Science*, *275*, 1–30. https://doi.org/10.2475/ajs.275.1.1

López Sánchez-Vizcaíno, V., Rubatto, D., Gómez-Pugnaire, M. T., Trommsdorff, V., & Müntener, O. (2001). Middle Miocene high-pressure metamorphism and fast exhumation of the Nevado-Filábride Complex, SE Spain. *Terra Nova*, *13*(5), 327–332.

Mancilla, F., Booth-Rea, G., Stich, D., Pérez-Peña, J. V., Morales, J., Azañón, J. M., et al. (2015). Slab rupture and delamination under the Betics and Rif constrained from receiver functions. *Tectonophysics*, *663*, 225–237. https://doi.org/10.1016/j.tecto.2015.06.028

Martínez-Martínez, J. M., & Azañón, J. M. (1997). Mode of extensional tectonics in the southeastern Betics (SE Spain): Implications for the tectonic evolution of the peri-Alborán orogenic system. *Tectonics*, *16*, 205–225.

Martínez-Martínez, J. M., Soto, J. I., & Balanyá, J. C. (2002). Orthogonal folding of extensional detachments: Structure and origin of the Sierra Nevada elongated dome (Betics, SE Spain). *Tectonics*, *21*.

Massonne, H.-J. (2014). Wealth of P–T–t information in medium-high grade metapelites: Example from the Jubrique unit of the Betic Cordillera, S Spain. *Lithos*, *208–209*, 137–157. https://doi.org/10.1016/j.lithos.2014.08.027

Menant, A., Jolivet, L., & Vrielynck, B. (2016). Kinematic reconstructions and magmatic evolution illuminating crustal and mantle dynamics of the eastern Mediterranean region since the late Cretaceous. *Tectonophysics*, *675*, 103–140. https://doi.org/10.1016/j.tecto.2016.03.007

Michard, A., Goffé, B., Bouybaouene, M., & Saddiqi, O. (1997). Late Hercynian–Mesozoic thinning in the Alboran domain: Metamorphic data from the northern Rif, Morocco. *Terra Nova*, *9*(4), 171–174. https://doi.org/10.1046/j.1365-3121.1997.d01-24.x

Michard, A., Negro, F., Saddiqi, O., Bouybaouene, M. L., Chalouan, A., Montigny, R., & Goffé, B. (2006). Pressure–temperature–time constraints on the Maghrebide mountain building: Evidence from the Rif–Betic transect (Morocco, Spain), Algerian correlations, and geodynamic implications. *Comptes Rendus Geoscience*, *338*, 92–114. https://doi.org/10.1016/j.crte.2005.11.011

Monié, P., Galindo-Zaldivar, J., Gonzalez-Lodeiro, F., Goffe, B., & Jabaloy, A. (1991). ^{40}Ar/^{39}Ar geochronology of Alpine tectonism in the Betic Cordilleras (southern Spain). *Journal of the Geological Society*, *148*, 289–297.

Monié, P., Torres-Roldán, R. L., & García-Casco, A. (1994). Cooling and exhumation of the Western Betic Cordilleras, ^{40}Ar/^{39}Ar thermochronological constraints on a collapsed terrane. *Tectonophysics*, *238*, 353–379.

Montel, J.-M., Kornprobst, J., & Vielzeuf, D. (2000). Preservation of old U–Th–Pb ages in shielded monazite: Example from the Beni Bousera Hercynian kinzigites (Morocco). *Journal of Metamorphic Geology*, *18*, 335–342. https://doi.org/10.1046/j.1525-1314.2000.00261.x

Negro, F., Beyssac, O., Goffe, B., Saddiqi, O., & Bouybaouene, M. L. (2006). Thermal structure of the Alboran Domain in the Rif (northern Morocco) and the Western Betics (southern Spain). Constraints from Raman spectroscopy of carbonaceous material. *Journal of Metamorphic Geology*, *24*, 309–327. https://doi.org/10.1111/j.1525-1314.2006.00639.x

Nijhuis, H. J. (1964). *Plurifacial Alpine metamorphism in the south-eastern Sierra de los Filabres south of Lubrín, SE Spain* (Ph.D. Thesis). Univ. van Amsterdam.

Pearson, D. G., & Nowell, G. M. (2004). Re-Os and Lu-Hf isotope Constraints on the origin and age of pyroxenites from the Beni Bousera peridotite Massif: Implications for mixed peridotite-pyroxenite mantle sources. *Journal of Petrology*, *45*, 439–455. https://doi.org/10.1093/petrology/egg102

Platt, J. P. (1986). Dynamics of orogenic wedges and the uplift of high-pressure metamorphic rocks. *The Geological Society of America Bulletin*, *97*(9), 1037–1053. https://doi.org/10.1130/0016-7606(1986)97<1037:doowat>2.0.co;2

Platt, J. P., Anczkiewicz, R., Soto, J. I., Kelley, S. P., & Thirlwall, M. (2006). Early Miocene continental subduction and rapid exhumation in the western Mediterranean. *Geology*, *34*, 981–984. https://doi.org/10.1130/g22801a.1

Platt, J. P., Argles, T. W., Carter, A., Kelley, S. P., Whitehouse, M. J., & Lonergan, L. (2003). Exhumation of the Ronda peridotite and its crustal envelope: Constraints from thermal modelling of a P–T–time array. *Journal of the Geological Society*, *160*, 655–676. https://doi.org/10.1144/0016-764902-108

Platt, J. P., Behr, W. M., Johanesen, K., & Williams, J. R. (2013). The Betic-Rif arc and its orogenic Hinterland: A review. *Annual Review of Earth and Planetary Sciences*, *41*, 313–357. https://doi.org/10.1146/annurev-earth-050212-123951

Platt, J. P., Kelley, S. P., Carter, A., & Orozco, M. (2005). Timing of tectonic events in the Alpujárride Complex, Betic Cordillera, southern Spain. *Journal of the Geological Society*, *162*, 451–462. https://doi.org/10.1144/0016-764903-039

Platt, J. P., Soto, J.-I., Whitehouse, M. J., Hurford, A. J., & Kelley, S. P. (1998). Thermal evolution, rate of exhumation, and tectonic significance of metamorphic rocks from the floor of the Alboran extensional basin, western Mediterranean. *Tectonics*, *17*, 671–689. https://doi.org/10.1029/98tc02204

Platt, J. P., Van den Eeckhout, B., Janzen, E., Konert, G., Simon, O. J., & Weijermars, R. (1983). The structure and tectonic evolution of the Aguilón fold-nappe, Sierra Alhamilla, Betic Cordilleras, SE Spain. *Journal of Structural Geology*, *5*(5), 519–538. https://doi.org/10.1016/0191-8141(83)90057-3

Platt, J. P., & Vissers, R. L. M. (1989). Extensional collapse of thickened continental lithosphere: A working hypothesis for the Alboran Sea and Gibraltar arc. *Geology*, *17*, 540. https://doi.org/10.1130/0091-7613(1989)017<0540:ecotcl>2.3.co;2

Platt, J. P., & Whitehouse, M. J. (1999). Early Miocene high-temperature metamorphism and rapid exhumation in the Betic Cordillera (Spain): Evidence from U–Pb zircon ages. *Earth and Planetary Science Letters*, *171*, 591–605. https://doi.org/10.1016/s0012-821x(99)00176-4

Plunder, A., Agard, P., Chopin, C., Soret, M., Okay, A. I., & Whitechurch, H. (2016). Metamorphic sole formation, emplacement and blueschist facies overprint: Early subduction dynamics witnessed by western Turkey ophiolites. *Terra Nova*, *28*, 329–339. https://doi.org/10.1111/ter.12225

Prada, M., Sallares, V., Ranero, C. R., Vendrell, M. G., Grevemeyer, I., Zitellini, N., & de Franco, R. (2018). Spatial variations of magmatic crustal accretion during the opening of the Tyrrhenian back-arc from wide-angle seismic velocity models and seismic reflection images. *Basin Research*, *30*, 124–141. https://doi.org/10.1111/bre.12211

Priem, H. N. A., Boelrijk, N. A. I. M., Hebeda, E. H., Oen, I. S., Verdurmen, E. A. T., & Verschure, R. H. (1979). Isotopic dating of the emplacement of the ultramafic masses in the Serrania de Ronda, Southern Spain. *Contributions to Mineralogy and Petrology*, *70*, 103–109. https://doi.org/10.1007/bf00371876

Puga, E., Fanning, M., Díaz de Federico, A., Nieto, J. M., Beccaluva, L., Bianchini, G., & Díaz Puga, M. A. (2011). Petrology, geochemistry and U–Pb geochronology of the Betic ophiolites: Inferences for pangaea break-up and birth of the westernmost Tethys Ocean. *Lithos*, *124*, 255–272. https://doi.org/10.1016/j.lithos.2011.01.002

Renne, P. R., Swisher, C. C., Deino, A. L., Karner, D. B., Owens, T. L., & DePaolo, D. J. (1998). Intercalibration of standards, absolute ages and uncertainties in $^{40}Ar/^{39}Ar$ dating. *Chemical Geology*, *145*(1–2), 117–152. https://doi.org/10.1016/s0009-2541(97)00159-9

Rossetti, F., Theye, T., Lucci, F., Bouybaouene, M. L., Dini, A., Gerdes, A., et al. (2010). Timing and modes of granite magmatism in the core of the Alboran Domain, Rif chain, northern Morocco: Implications for the Alpine evolution of the western Mediterranean. *Tectonics*, *29*. https://doi.org/10.1029/2009tc002487

Ruiz-Cruz, M. D., & Sanz de Galdeano, C. (2014). Garnet variety and zircon ages in UHP meta-sedimentary rocks from the Jubrique zone (Alpujárride Complex, Betic Cordillera, Spain): Evidence for a pre-Alpine emplacement of the Ronda peridotite. *International Geology Review*, *56*, 845–868. https://doi.org/10.1080/00206814.2014.904759

Sanchez, G., Rolland, Y., Schneider, J., Corsini, M., Oliot, E., Goncalves, P., & Marquer, D. (2011). Dating low-temperature deformation by 40Ar/39Ar on white mica, insights from the Argentera-Mercantour Massif (SW Alps). *Lithos*, *125*(1–2), 521–536. https://doi.org/10.1016/j.lithos.2011.03.009

Sánchez-Rodríguez, L., & Gebauer, D. (2000). Mesozoic formation of pyroxenites and gabbros in the Ronda area (southern Spain), followed by early Miocene subduction metamorphism and emplacement into the middle crust: U–Pb sensitive high-resolution ion microprobe dating of zircon. *Tectonophysics*, *316*, 19–44.

Santamaría-López, Á., Lanari, P., & de Galdeano, C. S. (2019). Deciphering the tectono-metamorphic evolution of the Nevado-Filábride complex (Betic Cordillera, Spain)—A petrochronological study. *Tectonophysics*, *767*, 128158.

Sanz de Galdeano, C., & López-Garrido, A. C. (1999). Nature and impact of the Neotectonic deformation in the western Sierra Nevada (Spain). *Geomorphology*, *30*(3), 259–272.

Scaillet, S. (1996). Excess ^{40}Ar transport scale and mechanism in high-pressure phengites: A case study from an eclogitized metabasite of the Dora-Maira nappe, western Alps. *Geochimica et Cosmochimica Acta*, *60*(6), 1075–1090. https://doi.org/10.1016/0016-7037(95)00440-8

Scaillet, S., Féraud, G., Ballèvre, M., & Amouric, M. (1992). MgFe and [(Mg, Fe) Si-Al2] compositional control on argon behaviour in high-pressure white micas: A $^{40}Ar/^{39}Ar$ continuous laser-probe study from the Dora-Maira nappe of the internal western Alps, Italy. *Geochimica et Cosmochimica Acta*, *56*(7), 2851–2872. https://doi.org/10.1016/0016-7037(92)90364-o

Serrano, F., de Galdeano, C. S., Kadiri, K. E., Guerra-Merchán, A., López-Garrido, A. C., Martín-Martín, M., & Hlila, R. (2006). Oligocene-early Miocene transgressive cover of the Betic-Rif internal zone. Revision of its geologic significance. *Eclogae Geologicae Helvetiae*, *99*, 237–253. https://doi.org/10.1007/s00015-006-1186-9

Serrano, F., Guerra-Merchán, A., El Kadiri, K., de Galdeano, C. S., López-Garrido, Á. C., Martín-Martín, M., & Hlila, R. (2007). Tectono-sedimentary setting of the Oligocene-early Miocene deposits on the Betic-Rifian internal zone (Spain and Morocco). *Geobios*, *40*, 191–205. https://doi.org/10.1016/j.geobios.2006.04.005

Simancas, J. F. (2018). A reappraisal of the Alpine structure of the Alpujárride Complex in the Betic Cordillera: Interplay of shortening and extension in the westernmost Mediterranean. *Journal of Structural Geology*, *115*, 231–242. https://doi.org/10.1016/j.jsg.2018.08.001

Simon-Labric, T., Rolland, Y., Dumont, T., Heymes, T., Authemayou, C., Corsini, M., & Fornari, M. (2009). $^{40}Ar/^{39}Ar$ dating of penninic front tectonic displacement (W Alps) during the lower Oligocene (31–34 Ma). *Terra Nova*, *21*(2), 127–136.
Sosson, M., Morrillon, A.-C., Bourgois, J., Féraud, G., Poupeau, G., & Saint-Marc, P. (1998). Late exhumation stages of the Alpujarride Complex (western Betic Cordilleras, Spain): New thermochronological and structural data on los Reales and Ojen nappes. *Tectonophysics*, *285*, 253–273. https://doi.org/10.1016/s0040-1951(97)00274-6
Soto, J. I., & Azañón, J. M. (1994). Zincian staurolite in metabasites and metapelites from the Betic-Cordillera (SE Spain). *Neues Jahrbuch für Mineralogie - Abhandlungen*, *168*, 109–126.
Soto, J. I., & Platt, J. P. (1999). Petrological and structural evolution of high-grade metamorphic rocks from the floor of the Alboran Sea basin, western Mediterranean. *Journal of Petrology*, *40*(1), 21–60. https://doi.org/10.1093/petroj/40.1.21
Spakman, W., Chertova, M. V., van den Berg, A., & van Hinsbergen, D. J. (2018). Puzzling features of western Mediterranean tectonics explained by slab dragging. *Nature Geoscience*, *11*(3), 211–216. https://doi.org/10.1038/s41561-018-0066-z
Spakman, W., & Wortel, R. (2004). A tomographic view on Western Mediterranean geodynamics. In W. Cavazza, F. M. Roure, W. Spakman, G. M. Stampfli, & P. A. Ziegler (Eds.), *The TRANSMED atlas—The Mediterranean region from crust to mantle* (pp. 31–52). Springer. https://doi.org/10.1007/978-3-642-18919-7_2
Steiger, R. H., & Jäger, E. (1977). Subcommission on geochronology: Convention on the use of decay constants in geo-and cosmochronology. *Earth and Planetary Science Letters*, *36*(3), 359–362. https://doi.org/10.1016/0012-821x(77)90060-7
Tagami, T., & Shimada, C. (1996). Natural long-term annealing of the zircon fission track system around a granitic pluton. *Journal of Geophysical Research*, *101*(B4), 8245–8255. https://doi.org/10.1029/95jb02885
Torres-Roldán, R. L. (1979). The tectonic subdivision of the Betic Zone (Betic Cordilleras, southern Spain); its significance and one possible geotectonic scenario for the westernmost Alpine Belt. *American Journal of Science*, *279*, 19–51.
Tubía, J., Cuevas, J., Navarro-Vilá, F., Alvarez, F., & Aldaya, F. (1992). Tectonic evolution of the Alpujárride complex (Betic cordillera, southern Spain). *Journal of Structural Geology*, *14*(2), 193–203.
Tubía, J. M. (1994). The Ronda peridotites (Los Reales nappe): An example of the relationship between lithospheric thickening by oblique tectonics and late extensional deformation within the Betic Cordillera (Spain). *Tectonophysics*, *238*, 381–398.
Tubía, J. M., Cuevas, J., & Gil Ibarguchi, J. (1997). Sequential development of the metamorphic aureole beneath the Ronda peridotites and its bearing on the tectonic evolution of the Betic Cordillera. *Tectonophysics*, *279*, 227–252.
Tubía, J. M., & Gil Ibarguchi, J. I. (1991). Eclogites of the Ojén nappe: A record of subduction in the Alpujárride complex (Betic Cordilleras, southern Spain). *Journal of the Geological Society*, *148*, 801–804.
Vergés, J., & Fernàndez, M. (2012). Tethys–Atlantic interaction along the Iberia–Africa plate boundary: The Betic–Rif orogenic system. *Tectonophysics*, *579*, 144–172.
Vissers, R. L. M., Platt, J. P., & van der Wal, D. (1995). Late orogenic extension of the Betic Cordillera and the Alboran domain: A lithospheric view. *Tectonics*, *14*, 786–803. https://doi.org/10.1029/95tc00086
Warren, C. J., Hanke, F., & Kelley, S. P. (2012). When can muscovite $^{40}Ar/^{39}Ar$ dating constrain the timing of metamorphic exhumation? *Chemical Geology*, *291*, 79–86. https://doi.org/10.1016/j.chemgeo.2011.09.017
Whitehouse, M. J., & Platt, J. P. (2003). Dating high-grade metamorphism—Constraints from rare-earth elements in zircon and garnet. *Contributions to Mineralogy and Petrology*, *145*, 61–74. https://doi.org/10.1007/s00410-002-0432-z
Wiederkehr, M., Sudo, M., Bousquet, R., Berger, A., & Schmid, S. M. (2009). Alpine orogenic evolution from subduction to collisional thermal overprint: The $^{40}Ar/^{39}Ar$ age constraints from the Valaisan Ocean, central Alps. *Tectonics*, *28*(6). https://doi.org/10.1029/2009tc002496
Zeck, H. P., & Whitehouse, M. J. (1999). Hercynian, Pan-African, Proterozoic and Archean ion-microprobe zircon ages for a Betic-Rif core complex, Alpine belt, W Mediterranean—Consequences for its P-T-t path. *Contributions to Mineralogy and Petrology*, *134*, 134–149. https://doi.org/10.1007/s004100050474
Zeck, H. P., & Whitehouse, M. J. (2002). Repeated age resetting in zircons from Hercynian–Alpine polymetamorphic schists (Betic–Rif tectonic belt, S. Spain)—A U–Th–Pb ion microprobe study. *Chemical Geology*, *182*, 275–292. https://doi.org/10.1016/s0009-2541(01)00296-0
Zeck, H. P., & Williams, I. S. (2001). Hercynian metamorphism in Nappe Core Complexes of the Alpine Betic–Rif Belt, western Mediterranean—A SHRIMP zircon study. *Journal of Petrology*, *42*, 1373–1385. https://doi.org/10.1093/petrology/42.7.1373

References From the Supporting Information

Aldaya, F., Alvarez, F., Galindo-Zaldívar, J., González-Lodeiro, F., Jabaloy, A. & Navarro-Villá, F. (1991). The Malaguide-Alpujarride contact (Betic Cordilleras, Spain): A brittle extensional detachment. *Comptes rendus de l'Académie des Sciences*, *313*, 1447–1453.
Aldaya, F., García-Dueñas, V., & Vilá, F. N. (1979). Los Mantos apujárrides del tercio central de las Cordilleras Béticas. Ensayo de la correlación tectónica de los Alpujárrides. *Acta Geologica Hispanica*.
Behr, W. M., & Platt, J. P. (2012). Kinematic and thermal evolution during two-stage exhumation of a Mediterranean subduction complex. *Tectonics*, *31*. https://doi.org/10.1029/2012tc003121
Blumenthal, M. M. (1927). Zum Bauplan betischer und penibetischer Decken im Norden der Provinz Málaga. *Geologische Rundschau*, *18*, 37–45. https://doi.org/10.1007/bf01802765
Bodinier, J. L., Morten, L., Puga, E., & Diaz de Federico, A. (1987). Geochemistry of metabasites from the Nevado-Filabride Complex, Betic Cordilleras, Spain: Relics of a dismembered ophiolitic sequence. *Lithos*, *20*, 235–245. https://doi.org/10.1016/0024-4937(87)90011-9
Booth-Rea, G., Martínez-Martínez, J. M., & Giaconia, F. (2015). Continental subduction, intracrustal shortening, and coeval upper-crustal extension: P-T evolution of subducted south Iberian paleomargin metapelites (Betics, SE Spain). *Tectonophysics*, *663*, 122–139. https://doi.org/10.1016/j.tecto.2015.08.036
Chalouan, A. (1986). *Les nappes Ghomarides (Rif septentrional, Maroc), un terrain varisque dans la chaîne alpine* (PhD Thesis). Univ. Louis Pasteur.
Chalouan, A., & Michard, A. (2004). The Alpine Rif Belt (Morocco): A case of mountain building in a subduction-subduction-transform fault triple junction. *Pure and Applied Geophysics*, *161*, 489–519. https://doi.org/10.1007/978-3-0348-7899-9_3
Chalouan, A., & Michard, A. (1990). The Ghomarides Nappes, Rif coastal range, Morocco: A Variscan chip in the Alpine Belt. *Tectonics*, *9*, 1565–1583. https://doi.org/10.1029/tc009i006p01565
Crespo-Blanc, A. (1995). Interference pattern of Miocene extensional systems in the Alpujarride Complex (N of Sierra Nevada, Betic Cordillera). *Geogaceta*, *17*, 140–142. https://doi.org/10.1016/0191-8141(95)e0044-d
Cuevas, J., Esteban, J. J., & Tubía, J. M. (2006). Tectonic implications of the granite dyke swarm in the Ronda peridotites (Betic Cordilleras, Southern Spain). *Journal of the Geological Society*, *163*, 631–640. https://doi.org/10.1144/0016-764905-038

Dyja, V. (2014). Interaction entre fluides de différents réservoirs lors de l'évolution d'un prisme orogénique en contexte de déformation partitionnée: Les Cordillères bétiques internes (Espagne). In *Implications sur le transfert de métaux dans la croûte. Ph.D. Thesis*. Univ. de Lorraine.

El Kadiri, K., Hlila, R., Sanz de Galdeano, C., López-Garrido, A. C., Chalouan, A., Serrano, F., et al. (2006). Regional correlations across the internides-externides front (northwestern Rif Belt, Morocco) during the late Cretaceous-early Burdigalian times: Palaeogeographical and palaeotectonic implications. *Special Publication-Geological Society of London*, *262*, 193–215. https://doi.org/10.1144/gsl.sp.2006.262.01.12

Esteban, J. J., Cuevas, J., Tubía, J. M., & Seward, D. (2004). Determinación de la naturaleza de la falla de Cerro Tajo (Macizo peridotítico de Carratraca) mediante termocronología de trazas de fisión. *Geogaceta*, *36*, 43–46.

Frasca, G., Gueydan, F., Brun, J.-P., & Monié, P. (2016). Deformation mechanisms in a continental rift up to mantle exhumation. Field evidence from the western Betics, Spain. *Marine and Petroleum Geology*, *76*, 310–328. https://doi.org/10.1016/j.marpetgeo.2016.04.020

Galindo-Zaldívar, J., Gonzalez-Lodeiro, F., & Jabaloy, A. (1989). Progressive extensional shear structures in a detachment contact in the Western Sierra Nevada (Betic Cordilleras, Spain). *Geodinamica Acta*, *3*, 73–85.

García-Dueñas, V., Balanyá, J. C., & Martínez-Martínez, J. M. (1992). Miocene extensional detachments in the outcropping basement of the northern Alboran Basin (Betics) and their tectonic implications. *Geo-Marine Letters*, *12*, 88–95.

García-Dueñas, V., Martínez, V., & Navarro-Vilá, F. (1986). *La zona de falla de Torres Cartas: Conjunto de fallas normales de bajo ángulo entre Nevado-Filabrides y Alpujarrides (Sierra Alhamilla, Béticas Orientales)*.

García-Dueñas, V., Martinez-Martinez, J. M., Orozco, M., & Soto, J. I. (1988). Plis-nappes, cisaillements syn-à post-métamorphiques et cisaillement ductiles-fragiles en distension dans les Nevado-Filábrides (Cordillères Bétiques, Espagne). *Comptes rendus de l'Académie des Sciences*, *307*, 1389–1395.

Garrido, C. J., Gueydan, F., Booth-Rea, G., Precigout, J., Hidas, K., Padrón-Navarta, J. A., & Marchesi, C. (2011). Garnet lherzolite and garnet-spinel mylonite in the Ronda peridotite: Vestiges of Oligocene backarc mantle lithospheric extension in the western Mediterranean. *Geology*, *39*, 927–930. https://doi.org/10.1130/g31760.1

Gómez de la Peña, M. T., & Fernàndez-Soler, J. M. (1987). High-pressure metamorphism in metabasites from the Betic Cordilleras (S.E. Spain) and its evolution during the Alpine orogeny. *Contributions to Mineralogy and Petrology*, *95*, 231–244.

Guerrera, F., Martin-Martin, M., Perrone, V., & Tramontana, M. (2005). Tectono-sedimentary evolution of the southern branch of the western Tethys (Maghrebian Flysch Basin and Lucanian Ocean): Consequences for western Mediterranean geodynamics. *Terra Nova*, *17*, 358–367. https://doi.org/10.1111/j.1365-3121.2005.00621.x

Gueydan, F., Pitra, P., Afiri, A., Poujol, M., Essaifi, A., & Paquette, J.-L. (2015). Oligo-Miocene thinning of the Beni Bousera peridotites and their Variscan crustal host rocks, Internal Rif, Morocco. *Tectonics*, *34*, 1244–1268. https://doi.org/10.1002/2014tc003769

Hebeda, E. H., Boelrijk, N. A. I. M., Priem, H. N. A., Verdurmen, E. A. T., Verschure, R. H., & Simon, O. J. (1980). Excess radiogenic Ar and undisturbed Rb-Sr systems in basic intrusives subjected to Alpine metamorphism in southeastern Spain. *Earth and Planetary Science Letters*, *47*, 81–90. https://doi.org/10.1016/0012-821x(80)90106-5

Jabaloy-Sánchez, A., Gómez-Pugnaire, M. T., Padrón-Navarta, J. A., López Sánchez-Vizcaíno, V., & Garrido, C. J. (2015). Subduction- and exhumation-related structures preserved in metaserpentinites and associated metasediments from the Nevado–Filábride Complex (Betic Cordillera, SE Spain). *Tectonophysics*, *644–645*, 40–57.

Jabaloy-Sánchez, A., Talavera, C., Gómez-Pugnaire, M. T., López-Sánchez-Vizcaíno, V., Vázquez-Vílchez, M., Rodríguez-Peces, M. J., & Evans, N. J. (2018). U-Pb ages of detrital zircons from the internal Betics: A key to deciphering paleogeographic provenance and tectono-stratigraphic evolution. *Lithos*, *318–319*, 244–266.

Kornprobst, J., & Durand-Delga, M. (1985). *Carte géologique du Rif au 1: 50.000* (Vol. 292). Feuille de Tétouan. Mém Serv Géol Maroc.

Kozur, H., Kampschuur, W., Mulder-Blanken, C. W. H., & Simon, O. J. (1974). Contribution to the triassic ostracode faunas of the Betic zone (southern Spain). *Scripta Geologica*, *23*, 1–56.

Lafuste, M. L. J., & Pavillon, M. J. (1976). Mise en evidence d'Eifélien daté au sein des terrains métamorphiques des zones internes des Cordillères Bétiques. Intérêt de ce nouveau repère stratigraphique. *Comptes rendus de l'Académie des Sciences*, *283*, 1015–1018.

Lenoir, X. (2001). The recrystallization front of the Ronda peridotite: Evidence for melting and thermal erosion of subcontinental lithospheric mantle beneath the Alboran Basin. *Journal of Petrology*, *42*, 141–158. https://doi.org/10.1093/petrology/42.1.141

Lonergan, L., & Platt, J. P. (1995). The Malaguide-Alpujarride boundary: A major extensional contact in the internal zone of the eastern Betic Cordillera, SE Spain. *Journal of Structural Geology*, *17*, 1655–1671. https://doi.org/10.1016/0191-8141(95)00070-t

López Sánchez-Vizcaíno, V., Gómez-Pugnaire, M. T., Garrido, C. J., Padrón-Navarta, J. A., & Mellini, M. (2009). Breakdown mechanisms of titanclinohumite in antigorite serpentinite (Cerro del Almirez massif, S. Spain): A petrological and TEM study. *Lithos*, *107*, 216–226.

López Sánchez-Vizcaíno, V., Trommsdorff, V., Gómez-Pugnaire, M. T., Garrido, C. J., Müntener, O., & Connolly, J. A. D. (2005). Petrology of titanian clinohumite and olivine at the high-pressure breakdown of antigorite serpentinite to chlorite harzburgite (Almirez Massif, S. Spain). *Contributions to Mineralogy and Petrology*, *149*, 627–646.

Marchesi, C., Garrido, C. J., Bosch, D., Bodinier, J.-L., Hidas, K., Padrón-Navarta, J. A., & Gervilla, F. (2012). A late Oligocene suprasubduction setting in the westernmost Mediterranean revealed by intrusive pyroxenite dikes in the Ronda peridotite (southern Spain). *The Journal of Geology*, *120*, 237–247. https://doi.org/10.1086/663875

Martín-Algarra, A. (1987). *Evolución geológica alpina del contacto entre las Zonas Internas y las Zonas Externas de la Cordillera Bética*. (PhD Thesis). Univ. de Granada.

Martínez-Martínez, J. M. (1986). *Evolucion tectono-metamorphuca del complejo Nevado-Filabride en el sector de union entre Sierra Nevada y Sierra de los Filabres (Cordilleras Beticas)* (Ph.D. Thesis). Univ. de Granada.

Mazzoli, S., & Martín-Algarra, A. (2011). Deformation partitioning during transpressional emplacement of a 'mantle extrusion wedge': The Ronda peridotites, western Betic Cordillera, Spain. *Journal of the Geological Society*, *168*, 373–382. https://doi.org/10.1144/0016-76492010-126

Mazzoli, S., Martín-Algarra, A., Reddy, S. M., Sánchez-Vizcaíno, V. L., Fedele, L., & Noviello, A. (2013). The evolution of the footwall to the Ronda subcontinental mantle peridotites: Insights from the Nieves unit (western Betic Cordillera). *Journal of the Geological Society*, *170*, 385–402. https://doi.org/10.1144/jgs2012-105

Michard, A., Chalouan, A., Feinberg, H., Goffé, B., & Montigny, R. (2002). How does the Alpine belt end between Spain and Morocco? *Bulletin de la Societe Geologique de France*, *173*, 3–15. https://doi.org/10.2113/173.1.3

Morten, L., Bargossi, G. M., Martinez, J. M. M., Puga, E., & Federico, A. D. (1987). Metagabbro and associated eclogites in the Lubrin area, Nevado-Filabride Complex, Spain. *Journal of Metamorphic Geology*, *5*, 155–174. https://doi.org/10.1111/j.1525-1314.1987.tb00377.x

Padrón-Navarta, J. A., Hermann, J., Garrido, C. J., López Sánchez-Vizcaíno, V., & Gómez-Pugnaire, M. T. (2010). An experimental investigation of antigorite dehydration in natural silica-enriched serpentinite. *Contributions to Mineralogy and Petrology*, *159*, 25–42.

Platt, J. P., Allerton, S., Kirker, A., Mandeville, C., Mayfield, A., Platzman, E. S. & Rimi, A. (2003). The ultimate arc: Differential displacement, oroclinal bending, and vertical axis rotation in the External Betic-Rif arc. *Tectonics*, *22*. Retrieved from http://doi.wiley.com/10.1029/2001TC001321

Platt, J. P., & Behrmann, J. H. (1986). Structures and fabrics in a crustal-scale shear zone, Betic Cordillera, SE Spain. *Journal of Structural Geology*, *8*, 15–33. https://doi.org/10.1016/0191-8141(86)90014-3

Priem, H. N. A., Boelrijk, N. A. I. M., Hebeda, E. H., & Verschure, R. H. (1966). Isotopic age determinations on tourmaline granite-gneisses and a metagranite in the eastern Betic Cordilleras (southeastern Sierra de los Filabres), SE Spain. *Geologie en Mijnbouw*, *45*, 184–187.

Puga, E., Díaz de Federico, A., Fanning, M., Nieto, J., Rodríguez Martínez-Conde, J., Díaz Puga, M., et al. (2017). The Betic ophiolites and the Mesozoic evolution of the western Tethys. *Geosciences*, *7*, 31. https://doi.org/10.3390/geosciences7020031

Renne, P. R., Swisher, C. C., Deino, A. L., Karner, D. B., Owens, T. L., & DePaolo, D. J. (1998). Intercalibration of standards, absolute ages and uncertainties in 40Ar/39Ar dating. *Chemical Geology*, *145*, 117–152. https://doi.org/10.1016/s0009-2541(97)00159-9

Rodríguez-Cañero, R., Jabaloy-Sánchez, A., Navas-Parejo, P., & Martín-Algarra, A. (2018). Linking palaeozoic palaeogeography of the Betic Cordillera to the Variscan Iberian Massif: New insight through the first conodonts of the Nevado-Filábride Complex. *International Journal of Earth Sciences*, *107*, 1791–1806.

Ruiz-Cruz, M. D., Sanz de Galdeano, C., & Santamaría, A. (2015). Petrology and thermobarometric estimates for metasediments, orthogneisses, and eclogites from the Nevado-Filábride Complex in the western Sierra Nevada (Betic Cordillera, Spain). *The Canadian Mineralogist*, *53*, 1083–1107. https://doi.org/10.3749/canmin.1500037

Scaillet, S. (2000). Numerical error analysis in $^{40}Ar/^{39}Ar$ dating. *Chemical Geology*, *162*, 269–298. https://doi.org/10.1016/s0009-2541(99)00149-7

Scaillet, S., & Guillou, H. (2004). A critical evaluation of young (near-zero) K–Ar ages. *Earth and Planetary Science Letters*, *220*, 265–275. https://doi.org/10.1016/s0012-821x(04)00069-x

Tubía, J. M., Cuevas, J., & Esteban, J. J. (2013). Localization of deformation and kinematic shift during the hot emplacement of the Ronda peridotites (Betic Cordilleras, southern Spain). *Journal of Structural Geology*, *50*, 148–160.

Tubía, J. M., Cuevas, J., & Esteban, J. J. (2004). Tectonic evidence in the Ronda peridotites, Spain, for mantle diapirism related to delamination. *Geology*, *32*, 941.

Tubía, J. M., Cuevas, J., Navarro-Vilá, F., Alvarez, F., & Aldaya, F. (1992). Tectonic evolution of the Alpujárride Complex (Betic Cordillera, southern Spain). *Journal of Structural Geology*, *14*, 193–203.

Zeck, H. P., Albat, F., Hansen, B. T., Torres-Roldán, R. L., Garciá-Casco, A., & Martín-Algarra, A. (1989). A 21 ± 2 Ma age for the termination of the ductile alpine deformation in the internal zone of the betic cordilleras, South Spain. *Tectonophysics*, *169*, 215–220. https://doi.org/10.1016/0040-1951(89)90196-0

Zeck, H. P., Kristensen, A. B., & Williams, I. S. (1998). Post-collisional volcanism in a sinking slab setting—Crustal anatectic origin of pyroxene-andesite magma, Caldear Volcanic Group, Neogene Alborán volcanic province, southeastern Spain. *Lithos*, *45*, 499–522. https://doi.org/10.1016/s0024-4937(98)00047-4